

Elastic and Viscoelastic Models of Crustal Deformation in Subduction Earthquake Cycles

Kelin Wang

Pacific Geoscience Centre, Geological Survey of Canada

9860 West Saanich Road, Sidney, British Columbia

KWang@nrcan.gc.ca

In The Seismogenic Zone of Subduction Thrust Faults, edited by T. Dixon and J. C. Moore, Columbia University Press, in press.

Abstract. An ideal model of subduction earthquake cycles that includes tectonic loading, rate-dependent friction, and viscoelastic stress relaxation is not yet available. For comparison with geodetic observations, the most widely used models treat fault motion in a purely kinematical fashion, that is, the fault slip (or state of locking) is estimated from surface observations regardless of the loading mechanism and frictional properties. These include forward and inverse elastic dislocation and viscoelastic models. Without addressing the loading mechanism, extra care should be taken to ensure that the assigned or estimated fault motion is physically valid. Time dependence is an important aspect of interseismic deformation, although it is often difficult to distinguish between contributions from time-dependent fault motion and from stress relaxation of the upper mantle. A brief review of modeling work for the Cascadia margin is provided to demonstrate the advantages and limitations of the elastic and viscoelastic models and to explain a number of practical issues. A finite element viscoelastic model is used to model the evolution of forearc crustal deformation since the 1700 great earthquake. Elastic models can also fit most of the Cascadia geodetic observations but by assuming that all deformation is due to current fault motion. The fault motion thus determined effectively includes a contribution from stress relaxation.

1. Introduction

A “subduction earthquake cycle” includes a great earthquake and subsequent strain accumulation that leads to the next event. Here the use of the word “cycle” by no means implies periodicity: neither the size of the earthquakes nor the duration of the interseismic interval between two events need be a constant. Ideally, a model of earthquake cycles should account for tectonic stress loading of the system, stress relaxation of the rock

medium in response to previous earthquakes and ongoing loading, and fault rupture as a frictional instability. Such a comprehensive model is not yet available.

The loading mechanism is rarely addressed in earthquake cycle models because many fundamental issues regarding driving forces, strength of plate boundary faults, and the coupling of long-term tectonic processes and short-term earthquake cycles are not known or poorly understood. Assigning a slip rate on one part of the fault to drive seismic and aseismic slip of another part does not really represent loading by tectonic forces (we often know the velocity boundary conditions, but seldom know the stress boundary conditions). Models based on rate- and state-dependent friction laws are useful in demonstrating how seismic fault slips may start and stop as a result of the interplay between fault frictional behavior and system rigidity [*Stuart, 1988; Marone and Saffer, 2005; Beeler, 2005*], although what parameters to use when applying these friction laws to subduction faults is not well known. For comparison with geodetic observations, however, the most widely used models treat the fault motion in a purely kinematical fashion, that is, surface deformation is predicted from given fault slip (or state of locking) regardless of the loading mechanism and friction properties. These are the models to be discussed in the present paper.

In this type of model, the motion of the subduction fault is usually decomposed into a steady subduction component and an earthquake perturbation component [*Savage, 1983*]. It is assumed that multiple earthquake cycles cause no net deformation, and any long-term net deformation is attributed to steady subduction. There are also models that mix earthquake cycles and steady subduction [e.g., *Matsu'ura and Sato, 1989; Cohen, 1994*]. Unless necessary to explore nonlinear coupling between the two processes, long-term deformation associated with steady subduction can be studied with separate deformation models. With steady subduction subtracted, a fully locked segment of the fault can be equivalently described as backward slip at the plate convergence rate, and the slip deficit becomes “backslip” (Figure 1a). Therefore, a sudden forward slip, representing an earthquake, and subsequent slow backslip, representing fault locking, constitute a basic earthquake cycle.

Slip of the seismogenic portion of the fault as a function of time is schematically illustrated in Figure 1b, including (upper panel) and excluding (lower panel) steady

subduction. Each vertical line segment, i.e., an instantaneous slip, represents an earthquake. The commonly assumed, idealized staircase function (thick line in the upper panel) depicts a pure stick-slip process. It is possible that aseismic slip occurs before, between, or after earthquakes, as illustrated by points 1, 2, and 3 on Figure 1b, respectively, but these scenarios are usually not considered in earthquake cycle models. The simplest way to account for some aseismic slip between earthquakes is to assume that the slip is at a constant slow rate and to remove it together with steady subduction (thin solid line in Figure 1b) [*e.g.*, *Zheng et al.*, 1996]. The effect is to reduce the amplitude of the saw-tooth slip function.

This review article consists of two parts. First, a critical review of the subject is provided (Section 2). Attention is paid to the clarification of various concepts. No effort is made to compile an exhaustive reference list. Second, a brief review of recent modeling work for the Cascadia subduction zone is provided (Section 3). The examples provide a perspective for understanding model results when the same data can be explained using either elastic or viscoelastic models. Comparison is made with other subduction zones that have had recent great earthquakes.

2. Deformation models with prescribed fault motion

2.1. Kinematics vs. driving force

Driving force, or tectonic loading, is often studied in subduction zone stress models [*Wang and He*, 1999] or long-term deformation models such as for the accretionary prism [*Davis et al.*, 1983]. In earthquake cycle models with prescribed fault motion, the driving force is not considered. In this section, I wish to make the point that while we deal with the kinematics of fault motion, we should pay attention to what the prescribed motion implies about the forces that drive the motion. For simplicity, only purely elastic models are used as examples.

Figure 2 shows horizontal velocities predicted by three simple 2-D models with different assumptions on the behavior of the most updip segment of the subduction fault. In one model (green), the most updip end of the fault is assigned the plate convergence rate (i.e., zero backslip) while the downdip zone is locked. The steady slip of the updip end in this model is highly questionable, because there is no driving force for it [*Wang*

and Dixon, 2004a,b]. In the presence of a locked zone, it is very unlikely that any part of the updip segment can slip at this rate in a sustained fashion. If the updip segment is weak because of unconsolidated sediments or high pore fluid pressure [Moore *et al.*, 2005], it may not have much shear stress and is not locked in a mechanical sense. This is represented by the model with a frictionless updip segment (red). The predicted surface velocities are similar to that predicted by assuming the fault to be locked all the way to the trench (black). Because of the presence of the downdip locked zone, this updip segment has little slip and, kinematically, it is better to consider it part of the “locked” zone. This reasoning is consistent with the lack of resolvable slip of the shallowest part of the subduction fault off Peru [Gagnon *et al.*, 2005].

If the updip segment has a stable frictional behavior, it may be pushed to slip when the locked zone ruptures in the next earthquake. If the updip segment does not slip during the earthquake or slips more slowly when the locked segment ruptures, compressive stress is increased in the upper plate above the two segments. The relief of this incremental stress (release of strain energy) can cause the updip segment to slip in a transient fashion while the downdip segment is locked, as observed after the M_w 8.7 2005 Nias-Simeulue, Sumatra, earthquake [Hsu *et al.*, 2006]. But it cannot slip if the stress is relieved. At a given point in time, we may see an updip segment slip faster than a downdip segment. However, slipping at the plate convergence rate is unlikely to last for a long time. The behavior of the velocity-strengthening updip segment in earthquake cycles is discussed in Wang and Hu [2006] in the context of critical and stable Coulomb wedges.

Many papers claim that inversion of inter-seismic land-based geodetic, mainly GPS, data has shown the updip edge of the subduction fault (offshore) to be slipping continuously at the convergence rate. Actually, the continuous slip was not “resolved” by geodetic data but was assigned as a boundary condition (zero backslip) in the inversion. GPS networks are usually too far from the trench to resolve this motion uniquely as shown in Figure 2.

A few other problematic backslip patterns are schematically shown in Figure 3 (left panels). Similar patterns are frequently seen in geodetic inversion results, and the patches with higher backslip rates are very often called “asperities”. For each pattern, the actual

slip distribution it represents is shown in the right panel. The slip vector of steady subduction is indicated using an arrow between the two panels. In Figure 3a, the backslip rate is faster than plate convergence, such that when steady subduction is added back, the fault actually slips backward. This pattern is surprisingly popular in the literature, but it represents an unlikely scenario in which a segment of a subduction thrust fault becomes a (aseismically slipping) normal fault. In Figure 3b, the backslip vector is at a significant angle with the direction of plate convergence. With steady plate motion added back, the actual slip of the fault segment is nearly perpendicular to plate convergence. Figure 3c is similar to Figure 3b but is a more common version of an “asperity”, with the backslip rate attaining a maximum value at the center of the patch. The backslip distribution appears quite reasonable, but it represents a very complex, if not unlikely, slip pattern if steady subduction is added back: The center of the asperity slips at a different direction from its surrounding areas. It is difficult to accept that the backslip patterns in Figures 3a, 3b, or 3c represent fault locking. Figures 3d and 3e show that a small fault patch between two locked patches slips by itself at the plate convergence rate (zero backslip rate). In reality, the slipping corridor in each of these two cases, similar to the updip segment in Figure 2, is unlikely to slip in a sustained fashion when its neighboring areas are locked.

Except perhaps for the first one, the scenarios in Figure 3 may be possible as transient phenomena under very special circumstances. One part of the subduction fault may occasionally slip aseismically in an odd fashion, especially in response to the rupture of neighboring fault patches. These scenarios require special explanations about their driving forces and do not represent general interseismic behavior. The least we can do (or the editors can request) is to avoid directly interpreting backslip patterns like the left panels of Figure 3. Adding back the removed steady-subduction motion as in the right panels of Figure 3 often immediately reveals problems.

2.2. Time-independent vs. time-dependant deformation

Numerous geological and geodetic observations have been made to constrain co-seismic and interseismic crustal deformation in response to the rupture and locking of subduction faults. It is generally not difficult to fit most of the data by adjusting parameters or performing an inversion. The challenge is to establish a first-order

deformation pattern from the data that allows us to explore the underlying physical processes.

When using a purely elastic model to study interseismic deformation and analyze hazard potential for future earthquakes, there is often a tacit assumption that interseismic deformation rate does not change with time. Some key observations tell us that the deformation rate is strongly time-dependent. Geodetic observations made at a given time, and to some extent the elastic models based on these observations, represent a “snapshot” of an evolving deformation field. Important characteristics of subduction earthquake-cycle deformation are schematically summarized in Figure 4, where the velocities and displacements are relative to distant regions of the upper plate that are not affected by the earthquake cycle.

1) At the co-seismic stage, most of the crustal deformation occurs near the rupture area, although deformation caused by very large events such as the $M_w \sim 9.2$ 2004 Sumatra earthquake can be detected at rather large epicentral distances [Chlieh *et al.*, 2006]. It is well known that the co-seismic deformation can be modeled using an elastic earth model. According to these models, maximum subsidence occurs roughly above the fault area in which the rupture zone tapers to zero in the downdip direction (point *a* in Figure 4). For active continental margins, if the coastline is around this area, geological evidence for past co-seismic subsidence can be observed [Plafker, 1972; Atwater, 1987; Atwater and Hemphill-Haley, 1997].

2) Within days to months following a subduction earthquake, deformation near the co-seismic rupture zone appears to be much faster than decades or centuries after. The fast post-seismic deformation was apparent in elevation changes inferred from tide gauge records after of the 1944/46 Nankai earthquakes [Thatcher and Rundle, 1984]. Similar post-seismic transients have been detected by continuously monitoring GPS networks in other subduction zones [Bürgmann *et al.*, 2001; Melbourne *et al.*, 2002; Yagi *et al.*, 2003].

3) Geological and geodetic observations made within a few years after great subduction earthquakes indicate that the region of maximum co-seismic subsidence quickly bounces back to become a region of uplift (point *b* in Figure 4). The observations include repeat leveling data before and after the 1944/46 great Nankai, SW Japan,

earthquakes [Thatcher, 1984] and comparison of tide gauge records after the 1964 great Alaska earthquake with *Plafker's* [1971] co-seismic deformation observations [Cohen and Freymueller, 2001].

4) With rare exceptions, GPS measurements at subduction zones show landward motion of coastal regions (point *c* in Figure 4), understood to reflect the interseismic locking of the subduction fault [e.g., Dixon, 1993; Norabuena et al, 1998]. However, at least for great earthquakes that rupture a very long segment of the margin such as the 1960 Mw = 9.5 Chile earthquake and the 1964 Mw = 9.2 Alaska earthquake, some inland areas 200 to 400 km from the trench still slowly move seaward a few decades after the event (point *d* in Figure 4), as if to slowly catch up with the co-seismic motion [Savage et al., 1999; Freymueller et al., 2000; Klotz et al., 2001; Khazaradze et al., 2002].

5) The only place where geodetic observations have spanned a nearly complete subduction earthquake cycle is the Nankai margin. Repeat leveling observations [Thatcher, 1984] show that vertical crustal deformation in response to the 1944/46 great earthquakes gradually spreads out from the rupture area, with the amplitude decreasing with time (point *e* in Figure 4). The pattern has been shown to be consistent with stress relaxation of the upper mantle after the earthquake [Thatcher and Rundle, 1984; Miyashita, 1987]. Horizontal strain observations that were made a few decades ago did not have sufficient accuracy to define the deformation history clearly, but by inference the evolution of horizontal deformation should be similar to that of the vertical deformation (point *f* in Figure 4).

6) One phenomenon not illustrated in Figure 4 is the recently discovered episodic silent slip events, presumably occurring along the subduction zone plate interface, especially downdip from the seismogenic zone. GPS networks have recently detected such slips in a number of places, the best examples including a few centimeters of slip over a couple of weeks at northern Cascadia [Dragert et al., 2001] and tens of centimeters of slip over a couple of years at eastern Nankai [Ozawa et al., 2002]. The Cascadia slip events show intriguing recurrence regularity and are accompanied by low-frequency non-volcanic seismic tremors [Rogers and Dragert, 2003]. The physical mechanism of these silent events and their implications to earthquake cycle models are currently under intense investigation.

In addition to the above main characteristics, there are significant differences between different subduction zones or different segments of the same subduction zone. The differences may be related to the age of the subducting plate, convergence rate, sediment thickness and type on the incoming plate, and subduction of special features such as seamounts or fossil and active spreading ridges, etc. A great earthquake may rupture only one segment of a subduction zone, and therefore different segments along the same margin may be at different stages of strain accumulation towards future earthquakes.

2.3. Linear vs. nonlinear mantle rheology

In the Maxwell viscoelastic rheology most frequently employed in geodynamic modeling, the rock material exhibits an instantaneous elastic behavior and longer-term viscous behavior. In response to fast loading such as an earthquake or rapid deglaciation, the deformation is initially elastic. The material gradually becomes more fluid like and eventually obeys a “steady-state” viscous flow law such as the following one.

$$\dot{\varepsilon} = A\sigma^n \exp\left(-\frac{Q}{RT}\right)$$

where $\dot{\varepsilon}$ is strain rate, and σ is stress, T is absolute temperature, A is a constant that may depend on grain size, Q is the activation energy, and R is the universal gas constant. The exponent n for mantle rocks depends on the microscopic deformation mechanism: $n = 1$ for diffusion creep and around 3 for dislocation creep. Conditions controlling the deformation mechanism have been discussed in *Karato and Wu* [1993]. Numerous deformation mechanisms at the microscopic scale result in various macroscopic flow laws [*Blenkinsop*, 2000], but the above power law is the most widely used in geodynamics. It is customary to quote flow laws for uniaxial shortening under axisymmetric compression, with $\dot{\varepsilon}$ being the shortening rate and σ the difference between the axial stress and the uniform stress normal to the axis.

The above flow law is a steady-state one because it is applicable to rock specimens that deform at a constant strain rate under a given loading stress in laboratories. Deformation behavior between the initial elastic response and the eventual steady-state flow is described by the transient rheology. During the transient phase, strain rate decreases from a large value to that of the steady state. For temperatures appropriate for

the lower crust and mantle, strain in the transient phase may follow t^m , with $1/3 < m < 2/3$ [e.g., Weertman and Weertman, 1975; Ranalli and Schloessin, 1989] or other forms. The transient deformation may also be described using the linearly Kelvin viscoelasticity [e.g., Pollitz, 2003; Pollitz et al., 2006] in which the strain follows $[1 - \exp(-t/\tau_K)]$, where τ_K is a time constant. The transient rheology is probably very important for post-seismic deformation, but parameters involved are poorly known. The following discussions are based on the untested assumption that the transient rheology can be ignored.

The above steady-state flow law can be cast into a more general expression of the following form [e.g., *Melosh*, 1980; *Wu*, 1992],

$$\dot{\varepsilon} = B \sigma_{II}^{n-1} \sigma$$

where $\dot{\varepsilon}$ and σ are components of strain rate and stress tensors, respectively, σ_{II} is the second stress invariant, and parameter B combines the contributions of A and T . An effective viscosity $\eta(n)$ can be defined as

$$\eta(n) = \frac{\sigma}{2\dot{\varepsilon}} = \frac{1}{2B\sigma_{II}^{n-1}}$$

Although we focus on the stress dependence of the effective viscosity in this discussion, it should be mentioned that the effective viscosity is affected by many other conditions. Above all, it depends strongly on temperature and hence depth, although nonlinear coupling between temperature and flow can usually be ignored for earthquake cycle models, so that a constant background geothermal field can be used. Addition of water significantly decreases viscosity [e.g., *Karato and Wu*, 1993], and fluids from dehydrating subducting slab may weaken materials along the plate interface. Water released from the slab may serpentinize the forearc mantle wedge [*Hyndman and Peacock*, 2003]. The rheology of serpentinites is relatively poorly known.

For linear Maxwell viscoelasticity, assumed in most viscoelastic earthquake-cycle and post-glacial rebound models, $n = 1$, and $\eta(1)$ is the Newtonian viscosity. Given suddenly imposed and fixed strain, the induced elastic stress relaxes with time. The time scale of the stress relaxation is characterized by a constant Maxwell time $\tau(1)$

$$\tau(1) = \frac{\eta(1)}{\mu} = \frac{1}{2B\mu}$$

where μ is the shear modulus. Within time $\tau(1)$, the solid exhibits mostly elastic behavior.

For the power-law rheology, there is a similar Maxwell time definition. *Melosh and Raefsky* [1983] showed that for post-seismic deformation, the power-law Maxwell time can be defined as

$$\tau(n) = \frac{1}{2B\mu\sigma_o^{n-1}}$$

where σ_o is some characteristic value of the stress perturbation due to the earthquake, and a convenient value to use is the average stress drop in the earthquake.

For the nonlinear rheology, the Maxwell time depends on the initial stress perturbation. Stress relaxation is faster if the earthquake has a greater stress drop. Because of the power law relation, the effective viscosity in the highly stressed area such as around the deep end of the rupture is locally decreased, allowing fast shear deformation. However, as the stress is relaxed and hence the effective viscosity increased, the deformation drastically slows down. Compared with the linear rheology, the power-law rheology is characterized by very fast initial deformation and much slower later deformation. *Melosh and Raefsky* [1983] showed that the patterns of surface deformation following a single dip slip earthquake are virtually the same for Newtonian and power-law mantle rheologies, except for their very different time dependence: Solution for a power-law system can be obtained from that of a Newtonian system by replacing normalized time $t/\tau(1)$ in the latter solution with $[t/\tau(n)]^{1/n}$.

The effective viscosity for power-law flow depends on the total stress (or strain rate). It can be shown [*Melosh*, 1980] that if the stress perturbation is much smaller than the background stress associated with mantle convection, its contribution to the effective viscosity can be neglected. The effective viscosity then depends only on the background stress and can be regarded as Newtonian when used to evaluate deformation associated with the stress perturbation. This reasoning may provide some justification for using a Newtonian mantle for post-glacial rebound analysis. An earthquake can generate shear stresses greater than the background stress around the rupture zone, and Newtonian viscosity, at least in the highly stressed region, may be a rather poor approximation. A few fault dimensions away from the rupture zone and/or many $\tau(n)$ after the earthquake, the stress perturbation may be sufficiently small to justify the use of a Newtonian viscosity.

Until recently, there were few post-seismic observations to help distinguish between the Newtonian and power-law mantle rheology. Rapid development of space-geodesy for crustal deformation monitoring has now allowed us to make accurate, high-density, and continuous near-fault observations. Consideration of the nonlinear rheology is therefore becoming necessary and practical. For example, geodetically observed time-varying crustal deformation rates after recent earthquakes in California led *Freed and Bürgmann* [2004] to propose that power-law rheology applies to the upper mantle in that region. They showed that if the post-seismic deformation is modeled using a Newtonian mantle, a much lower viscosity is required to explain observations within the first couple of months than that required to explain later observations. However, a linear transient rheology may also be used to explain these observations [Pollitz, 2003].

2.4. Fault slip vs. system stress relaxation

Variable crustal deformation rates in earthquake cycles have two primary sources. One is temporal variation of fault slip, and the other is viscoelastic stress relaxation in the rock medium, particularly in the upper mantle. Time-dependent fault slip is an intrinsic feature of the rate- and state-dependent friction laws [Scholz, 2002]. Viscoelastic mantle rheology best explains post-glacial rebound observations and has also been widely applied to earthquake deformation analyses.

Other processes that may become important under certain conditions include deformation due to pore fluid pressure evolution of poroelastic rock systems in response to earthquakes. The effect of poroelasticity on post-seismic deformation has been reported for continental earthquakes [*e.g.*, Peltzer *et al.*, 1998; Fialko, 2004]. Limited modeling results for subduction earthquakes indicate that the effect may be important around the center of the rupture area [Masterlark *et al.*, 2001]. Unless the rupture extends significantly landward of the coast, the effect is difficult to detect using land-based geodetic observations. Poroelasticity will not be further addressed here. Some aspects of its application to earthquake problems are discussed in a separate review article [Wang, 2004].

The two primary sources of time-dependent deformation rates are not mutually exclusive, but models developed for them usually are. Models that use rate-dependent

friction laws usually employ a purely elastic medium, and viscoelastic models usually ignore the friction laws. Besides numerical difficulties, one argument for this separation is timescale. It is thought that transient fault slip may be important at a timescale of months to years, but viscoelastic stress relaxation is important at a timescale of decades to centuries. The “afterslip” of a downdip extension of the rupture zone of the 1994 Sanriku-oki earthquake off NE Japan lasted for no more than two years [Uchida *et al.*, 2003] or even within 100 days after the earthquake [Yagi *et al.*, 2003]. Post-seismic transients of duration of hours to months in other subduction zones have been explained using the afterslip model [Thatcher and Rundle, 1984; Bürgmann *et al.*, 2001; Melbourne *et al.*, 2002]. For short time scales such as seconds to months, we usually assume a purely elastic medium. However, there is no obvious reason why transient fault slip cannot last longer than several years. For example, the “afterslip” model has been used to explain crustal deformation at the Chile and Alaska margins a few decades following great earthquakes [Barrientos *et al.*, 1992; Zweck *et al.*, 2002]. Conversely, if nonlinear rheology is considered, as discussed in Section 2.3, viscoelastic stress relaxation may also explain some of the short-term post-seismic transients [Freed *et al.*, 2006], as the power-law Maxwell time $\tau(n)$ can be as short as days and weeks. Application of transient rheology without invoking after slip or power law can also fit observations of short-term postseismic deformation [Pollitz *et al.*, 2006]. In a kinematical model, however, one may choose to allow arbitrary fault slip patterns to fit surface deformation data, as is done in most geodetic inversion work.

Most of the characteristics of time-dependent deformation in Figure 4 can be modeled either with time-variable fault slip or with viscoelastic stress relaxation, or a combination of the two. That is, the same deformation history may be explained in different ways. The nonuniqueness cannot always be removed by making more observations. The acceptance of a model is often based on other knowledge. If the mantle viscosity is higher than 10^{20} Pa s ($\tau(1) > 50$ years), a purely elastic model is not a bad approximation for earthquake recurrence intervals of a couple of hundred years. But there is consensus that mantle viscosity for active margins is around 10^{19} Pa s (Table 1), and for such a low viscosity stress relaxation should be considered. In some cases, the source of the deformation is too shallow to be mantle stress relaxation, so that fault slip becomes a better explanation. For

example, continuous near-trench GPS observations following the 2005 Nias-Simeulue earthquake can only be explained as indicating after slip of the fault segment updip of the coseismic rupture zone [Hsu *et al.*, 2006]. In other cases, the fault slip model is not favored because it requires the slip to occur at very large depth where the temperature and pressure condition makes distributed viscous deformation more likely. However, nonlinear rheology tends to localize deformation, and the distinction between aseismic slip of the fault plane and rapid power-law creep of a shear band along the fault zone may become obscure downdip of the rupture zone. Exactly how much of the surface deformation is due to fault slip and how much is due to viscoelastic stress relaxation will remain a subject of debate for a long time to come.

2.5. Co-seismic vs. inter-seismic fault slip

Purely stick-slip motion of the seismogenic zone of subduction faults is commonly assumed (thick line in Figure 1b). For example, for hazard analysis, the size of a future earthquake is often estimated by multiplying the plate convergence rate with the average recurrence interval of past earthquakes. Rather deterministic relationships between the size of earthquake slip and the length of interseismic intervals have been proposed, “time predictable” or “slip predictable”, depending on whether the length of an interseismic interval is assumed proportional to the slip of the preceding or ensuing earthquake [Shimazaki and Nakada, 1980]. Although simple and seemingly plausible, these relationships have not yet been substantiated by reliable observations [*e.g.*, Murray and Segall, 2002].

It is not clear if the seismogenic zone is indeed purely stick-slip or, in other words, if co-seismic slips in many earthquake cycles should sum up to the total amount of plate convergence over a long period of time. Total seismic slip estimated from moment release of subduction earthquakes appears to be less than the total plate convergence for many subduction zones [Pacheco *et al.*, 1993], although there are significant uncertainties in estimating slip from seismic moment, especially in the assumed downdip width of the rupture zone [Hyndman, this volume]. To balance the plate convergence budget, insufficient co-seismic slip has to be compensated by inter-seismic creep of the seismogenic portion of the fault. The frequently reported very slow inter-seismic slip of

subduction faults (usually called “partial coupling”) from fitting coastal GPS observations may pertain to this issue.

At present, we do not know how the seismogenic zone actually moves during the time between great earthquakes. The seismogenic zone is mostly offshore and difficult to monitor using land-based GPS networks. Recent seismological findings from the Northeast Japan subduction zone may shed some light [*Hasegawa et al.*, 2005]. *Matsuzawa et al.* [2002] and *Igarashi et al.* [2003] reported recordings of earthquakes that repeatedly rupture the same fault patches of about 0.1 to 1 km dimension with variable recurrence intervals of weeks to a few years. Assuming these patches to be little stick-slip islands (asperities) surrounded by a sea of aseismic slip, *Igarashi et al.* [2003] and *Uchida et al.* [2003] were able to use the cumulative co-seismic slips of repeating earthquakes at individual asperities to represent the total aseismic slip of their surrounding area in a given time window. They envisioned that at a given time the subduction fault is a mosaic of interspersed large areas of little or no slip and regions of mostly aseismic slip that include the small repeating earthquakes. It is reasonable to speculate that the mosaic distribution is present at all scales (Figure 5). A group of closely spaced small asperities may form a large asperity, and a collection of these groups constitutes an even larger asperity, and so on. More widely spaced small asperities or groups of asperities surrounded by slipping regions may move in a stick-slip mode to produce repeating earthquakes. The distribution pattern may evolve with time, as influenced by earthquake rupture, pore fluid pressure, and fault zone materials, etc.

When developing an earthquake cycle model for a specific subduction zone, we usually have to assume a co-seismic slip without knowing how much inter-seismic slip actually takes place. In other words, we are not too sure which of the two saw-tooth functions in Figure 1b should be used. Most multiple-cycle models with prescribed fault slips suffer from this uncertainty. It is important to remember this uncertainty when using model results.

2.6. Forward modeling vs. inversion

Tarantola and Valette [1982, p.219] succinctly explained the nonuniqueness of inverse problems: “There are two reasons for nonuniqueness. In some problems the

nonuniqueness comes from the fact that the data are discrete; if the data are dense, the solution would be unique ... In other problems, nonuniqueness may be deeper, as, for example, in the inverse problem of obtaining the density structure of a region of the earth from the measurements of the local gravitational field: Gauss' theorem states that an infinity of different density configurations give identical gravitational fields."

The problem of determining fault slip from surface deformation data suffers from both sources of nonuniqueness. An inversion method can allow additional information to be incorporated in a mathematically rigorous manner. The additional information can be added explicitly as constraints such as a priori values, bounds, smoothness criteria, and "regularization" factors used to cure solution instability, or it can be added implicitly when an inverse problem is "parameterized". A simple example of parameterization is to divide a fault into a few patches of uniform slip, which reduces the number of unknown slip vectors from infinity to the number of fault patches. The fewer patches one uses, the "better resolved" (smaller error bars) are the slip vectors, simply because more information about the slip distribution has been assumed in the inversion. The error introduced in the parameterization is usually not formulated into the error bars of the resolved parameters.

Additional information is the key to the solution of any inverse problem. For this reason, inversion results are always influenced by the researcher's own understanding of the problem. Therefore it is normal to see different researchers obtain different results by using different inversion schemes or even by using the same scheme. This is not to say that inversion is the same as trial-and-error based forward modeling. Given all the information, a properly performed inversion does yield the most probable estimate of the parameter values, with an error bar representing the range of other possible, but less probable, solutions allowed by the same data. A more difficult question is: Is this best mathematical solution the best geophysical solution?

To perform an inversion, we assume that the system can be described by a set of physical laws, expressed in the form of mathematical equations. When the equations accurately describe the real physics, generally believed to be the case for static co-seismic deformation and seismic wave propagation, inversion may indeed yield the best geophysical solution. However, for problems like post-seismic and inter-seismic

deformation, the processes are much less well understood. We probably have to deal with poorly known processes more than just poorly known parameters. Deciding what processes to include and to neglect is the real challenge. The importance of reasoning, judgment, and intuition often outweighs that of statistical measures of data fit. In this case, forward modeling allows more flexibility in testing various processes and parameters and evaluating competing conceptual models. The usefulness of inverse methods will increase with the maturity level of the subject.

3. Cascadia Models

3.1. Geodetic observations

At the Cascadia subduction zone, the Juan de Fuca (JDF) plate subducts beneath the North America (NA) plate. The last great subduction earthquake at this margin occurred in 1700 with an estimated moment magnitude of 9 [Satake *et al.*, 2003]. The southern Cascadia forearc, primarily the relatively mafic Siletzia terrane in southern Washington and Oregon and the Klamath Mountains in northern California, moves northward toward the Canadian coast mountains (Figure 6) [Wells *et al.*, 1998; Wells and Simpson, 2001]. Its motion relative to the rest of North America can be described as a rigid forearc sliver rotating around an Euler pole. The position of this Oregon Coast – North America (OC-NA) pole as defined by Wells and Simpson [2001] is shown in Figure 6. There are questions regarding the presence of an eastern boundary of the forearc block [McCaffrey, 2002], but the questions do not concern the deformation of the coastal area in Cascadia great earthquake cycles.

Geodetic strain rates and GPS velocities along the Cascadia forearc are summarized in Figures 7a and 7b, respectively. The velocities are relative to reference GPS site DRAO in British Columbia (shown in Figure 6). Some of the strain rates in Figure 7a (blue crosses) were derived from the GPS data of Figure 7b. Sources for most of the strain rate data were reviewed in Wang *et al.* [2003], but Figure 7a displays an additional eight strain rate values in Oregon and southern Washington derived by McCaffrey [2002] from a larger campaign GPS data set. Campaign GPS velocities in Canada were reported by Henton [2000] and Mazzotti *et al.* [2003], and those in the U.S. by McCaffrey *et al.* [2000] and Savage *et al.* [2000]. Velocities at continuously monitoring GPS stations were

determined at the Pacific Geoscience Centre [Mazzotti *et al.*, 2003] and at the Central Washington University (M. Miller, personal communication, 2003). The strain rates in Figure 7a represent interseismic elastic strain buildup due to the locking of the subduction fault. There are two contributions to the GPS velocities, namely interseismic deformation and long-term forearc motion shown in Figure 6. For example, as coastal Oregon rigidly translates northward (Figure 7b), it is being elastically shortened in the E-W direction at the same time (Figure 7a).

For forearc deformation in earthquake cycles, it is the JDF-forearc not JDF-NA convergence that should be considered. By subtracting the OC-NA motion of Figure 6, we obtain the “corrected” GPS velocities in Figure 7c that represent crustal deformation in response to earthquake cycles. The northern forearc is not affected by the OC motion [Wells *et al.*, 1998], and therefore the JDF-forearc convergence in this region is just the JDF-NA convergence. The transition from the JDF-OC convergence in southern Cascadia to JDF-NA convergence in northern Cascadia is assumed to take place linearly over the area between the two dashed lines in Figure 7c [Mazzotti *et al.*, 2002].

There is a great deal of uncertainty in the long-term forearc motion. However, the removal of the rigid-body motion does not affect strain rates (Figure 7a) that were derived locally over small networks. The strain rate data and the northern-Cascadia GPS data that are not affected by the sliver correction provide primary constraints for the contemporary inter-seismic deformation of the Cascadia forearc. Vertical deformation data such as leveling, gravity, and tide-gauge measurements provide ground tilt information [Hyndman and Wang, 1995; Flück *et al.*, 1997], but they are best regarded as corroborative information because of a number of unresolved interpretation and observation issues [Wang *et al.*, 2003; Wolyneec, 2004].

3.2. Elastic half-space dislocation models

Two-dimensional (2-D) elastic dislocation models were used to model pre-GPS geodetic data for a few margin-normal profiles [Savage *et al.*, 1991, 2000; Hyndman and Wang, 1993, 1995; Dragert *et al.*, 1994]. The objective was to define the currently locked patch of the subduction fault. How the locked zone is terminated at its downdip end is not known, but we know the termination cannot be abrupt. So a zone of transition from full

locking (modeled as backslip at plate convergence rate) to slipping at plate convergence rate (modeled as zero backslip) was assumed. For a 2-D model (zero along-strike strain) assuming a uniform elastic half space, the results are independent of elastic moduli. For a 3-D half space, the results depend only on the Poisson's ratio, which is usually taken to be 0.25.

Geodetic data could allow a wider locked zone with a narrower transition zone or a narrower locked zone with a wider transition zone. *Hyndman and Wang* [1993, 1995] argued that the updip and downdip ends of the locked zone could be marked by temperatures of about 125°C and 350°C, respectively, and developed thermal models to determine these temperature along the subduction fault. They defined the donwdip limit using the thermal results but found that the Cascadia subduction fault was too warm to apply the updip limit. The 3-D dislocation model of *Flück et al.* [1997] was an extension of the 2-D model of *Hyndman and Wang* [1995] but included a more realistic curved subduction fault. Variations of this 3-D model were applied to smaller regions along the Cascadia margin [*Khazaradze et al.*, 1999; *Henton*, 2000].

A more recent 3-D dislocation model, called CAS3D-2, was published by *Wang et al.* [2003]. The model fault geometry and results are shown in Figures 8a and 9, respectively. The model was constrained primarily by strain rate data and northern-Cascadia GPS data. Other GPS data and vertical deformation data were used to validate the model. In addition to using substantially different observational constraints and removing the secular forearc motion (Figure 6), *Wang et al.* [2003] re-evaluated the concept of the transition zone. As discussed in Section 2.2, crustal deformation in earthquake cycles has a strong time dependence due to transient and episodic fault slip and viscoelastic stress relaxation. As explained in Section 2.4, it is often possible to find an equivalent fault slip distribution to model the effect of stress relaxation. Since elastic models can only deal with fault slip, such an equivalent approach becomes necessary.

The transition zone in CAS3D-2 and in many other elastic dislocation models serves to account for the viscoelastic effects that cannot be modeled with elastic models and for this reason is called the “effective transition zone” [*Wang et al.*, 2003]. Like the “effective elastic thickness” of the lithosphere, the “effective transition zone” characterizes integrated effects of many controlling factors using a single quantity. The

effective transition zone in the CAS3D-2 model has a backslip distribution that decreases in the downdip direction following an exponential function. Assuming a thermally controlled locked zone as in *Hyndman and Wang* [1995], *Wang et al.* [2003] adjusted the width of the effective transition zone and a parameter that controls the exponential shape of its backslip distribution to fit geodetic observations. The model applies to Cascadia crustal deformation 300 years after a great earthquake. If a dislocation model were to be developed for deformation earlier in the earthquake cycle, a much narrower effective transition zone would be needed.

There are other types of elastic models for Cascadia interseismic deformation. *Williams and McCaffrey* [2001] used a 2-D elastic plate model to represent the upper plate. A basal traction is used to resist the landward push by the subducting plate across the locked subduction fault. The role of the traction force is similar to that of the effective transition zone and can be adjusted to account for the effect of stress relaxation in the underlying mantle. 3-D inverse models were developed by *McCaffrey et al.* [2000] and *McCaffrey* [2002] to determine backslip distribution and forearc block rotation at the same time. *Yoshioka et al.* [2005] applied a 3-D inversion scheme to northern Cascadia GPS data. Inversion results tend to give greater variations in backslip distribution and some slow slip of the locked zone. As discussed in Section 2.5, differences between different models are due mostly to how the models are constrained and parameterized. For example, *McCaffrey* [2002] allowed significant on-going slow slip of the seismogenic zone off Oregon to fit the GPS data, but strain rates (not affected by block rotation) derived from the same data can be well explained by CAS3D-2 that assumes full locking (Figure 9a).

3.3. Viscoelastic models

The reason for pursuing viscoelastic models at Cascadia is to establish a connection between the 1700 great earthquake and contemporary geodetic deformation. Many parameters in viscoelastic deformation of the earth are poorly known, but we wish to know whether the available models can explain what we know about the 1700 earthquake and current crustal deformation and, if not, what additional data and/or assumptions are needed. The finite element method has been used for this type of model at Cascadia

because of its flexibility in dealing with geological structure such as a dipping elastic slab. The presence or absence of a slab makes a difference to the stress relaxation process [Miyashita, 1987]. A 2-D viscoelastic model was developed for northern Cascadia [Wang *et al.*, 1994]. 3-D Cartesian models were developed for the entire subduction zone for different plate convergence scenarios [Wang *et al.*, 2001]. In this article, we present some preliminary results of an ongoing modeling effort using spherical earth geometry and 27-node iso-parametric tri-quadratic finite elements. The effect of gravity is simulated using a pre-stress advection term [Wang *et al.*, 2001]. More detailed descriptions of the modeling technique and model results will be presented elsewhere.

3.3.1. Structure and Fault Slip

The basic structure of the model is schematically illustrated in Figure 10. Material properties for the preferred model are given in Table 2. Newtonian viscosities are assumed, and the values will be discussed separately in Section 3.3.3. The finite element mesh of the new model is shown in Figure 11. We use thicknesses of 40 km and 30 km for the overriding and subducting plates, respectively. The plate geometry is the same as in the 3-D Cartesian viscoelastic model of Wang *et al.* [2001]. The shallowest part (< 50 km depth) of the plate interface is also the same as in the elastic CAS3D-2 model. The construction of this type of models involves many simplifying assumptions. A very complex model would not reduce the number of assumptions but would introduce many more parameters and make it very difficult to evaluate the results.

For the rupture zone, the forward slip is calculated as the JDF-forearc convergence rate (discussed in section 3.1) times 500 years, a rough average of the recurrence interval of Cascadia subduction earthquakes. The prescribed slip linearly decreases to zero over a zone of transition that is much narrower than that of CAS3D-2 (Figure 8b). Although the seismic slip takes place in a single time step in the model, the linear transition is meant to account for some rapid post-seismic afterslip. Overlapping with the transition zone and further downdip is a viscoelastic layer of 1 km thickness that allows for continued slow slip after the earthquake. Details of the short-term post-seismic transients have little impact on the results 300 years after the earthquake. The JDF-forearc convergence rate and direction vary along strike (Figure 7c), and the forward slip thus calculated varies

accordingly. The along-strike average of the co-seismic slip is about 19 m. After the earthquake step, the rupture zone becomes the locked zone and is assigned a backslip at the plate convergence rate and direction to represent complete locking.

3.3.2. Results for the Preferred Model

The co-seismic slip distribution described above is exactly the same as in the half-space elastic dislocation model used to provide initial seafloor deformation for a trans-Pacific tsunami model for the 1700 earthquake [*Satake et al.*, 2003]. Predicted co-seismic deformation, not displayed here, is nearly identical to that shown in *Sakate et al.* [2003]. Variable elastic moduli in the finite element model only result in very small differences in the predicted surface deformation. *Satake et al.* [2003] has compared the model co-seismic deformation and resultant tsunami heights with geological observations and Japanese historical tsunami descriptions. New insights from the viscoelastic model are in the time dependence of crustal deformation.

Model deformation 50 years and 300 years after the earthquake are shown in Figures 12 and 13, respectively, with the 300-year results compared with modern geodetic observations. Velocities are shown only at continuous GPS stations. Results within 100 km of the northern and southern ends of the subduction zone should be interpreted with caution, because the model is not designed to model deformation around triple junctions. The model reproduces the first-order characteristics of time-dependent crustal deformation in subduction zone earthquake cycles summarized in Figure 4 and fits the modern geodetic data reasonably well. The model predicts that strain rates and uplift rates are expected to decrease with time. It also shows that at an early stage of interseismic deformation, such as 50 years, although coastal sites all move landward as a result of fault locking, the inland area is still moving seaward in the direction of co-seismic slip (Figure 12b).

3.3.3. Viscosities

The most critical yet uncertain parameter controlling the time-dependent deformation is the viscosity of the upper mantle. Post-glacial rebound models and subduction zone deformation models usually assume a linearly Maxwell mantle (but see Section 2.3).

Continent-scale post-glacial rebound models are constrained by data from the continental interior, and viscosities of $10^{21} - 10^{22}$ Pa s estimated from these models are probably not applicable to active margins. Viscosity values used in subduction zone viscoelastic deformation models are consistently lower (Table 1). Post-glacial rebound studies at the northern Cascadia margin yield a mantle viscosity of about 10^{19} Pa s [James *et al.*, 2000; Clague and James, 2002]. This is the value we have adopted for the continental upper mantle in our model. The relatively low value may be related to the addition of fluids released from the subducting slab.

Different from our previous model [Wang *et al.*, 2001], a value of 10^{20} Pa s is used for the oceanic mantle in the new model. We found that a smaller value would not produce the third characteristic of the time-dependent deformation discussed in Section 2.2, that is, the region of maximum co-seismic subsidence quickly becomes a region of fastest uplift. This effect is illustrated in Figure 14, which shows uplift histories at a location near the Washington coast (indicated by a green dot on the uplift-rate maps of Figures 12c and 13c) predicted by two models with different oceanic mantle viscosities. Co-seismic subsidence (at time zero) is not affected by the viscosity value. With a viscosity of 10^{19} Pa s for the oceanic mantle, the site will continue to subside after the earthquake for several decades. With a value of 10^{20} Pa s, the site reverses the sense of vertical motion immediately after the earthquake. That the oceanic mantle has a higher viscosity than the continental mantle wedge may reflect the lack of additional fluids due to slab dehydration.

Instead of a higher viscosity for the oceanic mantle, we may produce the immediate post-seismic uplift in the same area by assuming aseismic fault slip at depths greater than 30 km. We have already lumped the possible short-term afterslip into the co-seismic transition zone (Section 3.3.1), but a deeper afterslip that lasts longer in time cannot be ruled out. No relevant data are available at Cascadia to constrain the short-term post-seismic deformation.

3.3.4. Comparison With the Chile and Nankai Margins

The most important aspect of viscoelastic deformation in subduction earthquake cycles is the role of stress relaxation in the continental mantle wedge. The co-seismic

fault slip stretches the upper-plate forearc in the seaward direction. At this time, the entire system behaves elastically, and elastic shear stress is generated in the mantle wedge to resist the seaward stretch. This is why co-seismic crustal deformation is limited to the proximity of the rupture area. The stress relaxes after the earthquake. A lower viscosity leads to a faster relaxation. The stress relaxation allows the deformation in the upper plate to spread out, as is obvious in the evolution of the uplift rate pattern in Figures 12c and 13c. For earthquakes that rupture very long segments of the subduction fault, the stress relaxation also allows the inland area to move seaward slowly, to catch up with the seaward co-seismic motion of the forearc (point *d* in Figure 4).

Seaward motion of inland sites a few decades after a great earthquake has indeed been observed at the Chile and Alaska margins, as discussed in Section 2.2. A 3-D viscoelastic model [Hu *et al.*, 2004] similar to the Cascadia model explains the GPS observations 35 years after the 1960 great Chile earthquake very well. The successful application of the viscoelastic stress relaxation model to the Chile data lends support to the Cascadia model. For Alaska, Zweck *et al.* [2002] explained the present-day seaward motion of inland GPS sites by proposing an afterslip that lasted at least for several decades in a purely elastic Earth model. But Sato *et al.* [2003] showed that some viscoelastic stress relaxation is also required to explain these observations.

The Cascadia and the Nankai, SW Japan, margins are very similar in many ways [Wang, 2000], but modern strain rates derived from GPS observations at the Nankai forearc [e.g., Kato *et al.*, 1998] are larger than those at Cascadia. Part of the reason is that the Cascadia locked zone is generally farther offshore, but the contrast between Figures 12a and 13a adds another perspective. The most recent great earthquakes at Nankai occurred in 1944 (Mw = 8.2) and 1946 (Mw = 8.2), much more recent than the 1700 Cascadia event. The viscoelastic model indicates that the strain rates several decades after the earthquake should be larger than those 300 years after. The strain rate decrease with time due to stress relaxation is partially responsible for the difference in the strain-rate size between Nankai and Cascadia. If stress relaxation is not considered, this difference will have to be explained entirely using different fault locking scenarios (i.e., backslip distributions).

The along-strike rupture lengths of the 1944 and 1946 Nankai events are approximately 100 and 200 km, respectively, in contrast to the about 1000 km long ruptures of the 1960 Chile, 1964 Alaska, and 1700 Cascadia earthquakes. The shorter rupture perhaps explains why seaward motion similar to the Chile and Alaska margins is presently not observed at Nankai. Numerical experiments by *Hu et al.* [2004] show that such a short rupture will not result in significant seaward motion of the inland area a few decades after the earthquake, because it induces significant co-seismic shear stress in a much smaller region of the upper mantle. Shorter ruptures also tend to have smaller co-seismic slip and therefore, even near the rupture zone, cause less stress perturbation.

4. Summary

This article has focused on subduction zone earthquake cycle models with fault motion kinematically assigned (in forward modeling) or determined (in inverse modeling). For deformation of very short time scales, the earth material exhibits elastic behavior. Elastic models, even with the assumption of a uniform half space, generally describe co-seismic deformation and short-term post-seismic and inter-seismic deformation transients very well. For decadal and longer time scales, such as interseismic deformation and post-glacial rebound, the earth material, especially that of the upper mantle, exhibits viscoelastic behavior. The process of interseismic crustal deformation is poorly understood. Linear Maxwell viscoelasticity with a viscosity value of around 10^{19} Pa s is commonly used for subduction earthquake cycle models, but there are large uncertainties in the assumed rheology.

A critical review of earthquake cycle modeling is provided in the first half of this article. The main points of emphasis are summarized as follows.

(1) Because the driving force for fault slip is not considered in the backslip-type modeling, it is easy to come up with inter-seismic fault slip patterns that are unphysical or unlikely. The physical meaning of the backslip patterns used to fit geodetic data, especially those determined by inversion, should be carefully examined before inferences on fault properties and loading processes are made.

(2) Crustal deformation in subduction earthquake cycles is strongly time dependent, especially in the first few decades after a great earthquake. Co-seismic deformation is

limited near the rupture zone, with maximum subsidence occurring above the downdip end of the rupture, often around the coast. Rapid deformation within days to months of an earthquake (post-seismic transients) occurs in the proximity of the co-seismic rupture, but later inter-seismic deformation involves a wider area in the trench-normal direction. The zone of co-seismic subsidence quickly becomes the zone of fast uplift after the earthquake. For earthquakes with large rupture lengths along strike, the inland area a few hundred kilometers from the trench may continue to move seaward decades after the earthquake.

(3) Viscous deformation following an earthquake may follow the power law and/or be affected by the transient rheology. Linear (stress-independent) viscosity in viscoelastic earthquake cycle models is arguably a reasonable approximation for areas away from the fault rupture and sufficiently long after the earthquake. Much effort is needed to investigate the role of nonlinear and transient rock rheology.

(4) The timescale of post-seismic fault slip around the rupture zone, particularly the downdip segment, appears to be short. The same time-dependent surface deformation can often be explained by either time-dependent fault slip or viscoelastic stress relaxation. Additional knowledge is required to alleviate the nonuniqueness.

(5) The commonly assumed purely stick-slip motion of the seismogenic zone may not be valid for many subduction zones. How the seismogenic zone moves between great earthquakes deserves great future attention.

(6) The purpose of inversion is to determine parameters. Inverse methods are best applied to processes are relatively well understood, such as co-seismic deformation and seismic wave propagation. Forward modeling is needed to test conceptual models for poorly known processes such as interseismic deformation.

The second part of the article presents a brief review of the earthquake cycle modeling work conducted for the Cascadia subduction zone. Various models can be used to fit modern geodetic observations. Elastic models can be viewed to some degree as snapshots of time-dependent deformation. The slip distribution along the fault effectively accounts for the effect of viscoelastic stress relaxation. A viscoelastic model that assumes a Newtonian viscosity value of 10^{19} Pa s for the continental mantle and 10^{20} Pa s for the oceanic mantle yields a deformation history since the 1700 great earthquake that

reproduces all the primary features of interseismic deformation observed at different subduction zones. The model is also in general agreement with modern strain rate, GPS, and tide gauge observations in the Cascadia forearc. Although the model is specifically for the Cascadia subduction zone, the results are useful for understanding deformation patterns in other subduction zones. For example, the higher strain rates currently observed at the Nankai forearc and the seaward motion of inland GPS stations at the Chile and Alaska margins are consistent with model predicted deformation patterns several decades after a great earthquake.

Acknowledgements. J. He developed the computer program and carried out most of the simulation for the 3-D viscoelastic finite element model. Comments from B. Atwater, T. Dixon, R. D. Hyndman, W. Thatcher, and an anonymous reviewer substantially improved the article. Geological Survey of Canada contribution 2004098.

References

- Atwater, B. F. (1987), Evidence for great Holocene earthquakes along the outer coast of Washington State, *Science*, *236*, 942-944.
- Atwater, B. F., and E. Hemphill-Haley (1997), Recurrence intervals for great earthquakes of the past 3500 years at northeastern Willapa Bay, Washington, *U.S. Geological Survey Professional Paper*, *1576*, 108 pp.
- Barrientos, S. E., G. Plafker, and E. Lorca (1992), Postseismic coastal uplift in southern Chile, *Geophys. Res. Lett.*, *19*, 701-704.
- Beeler, N. M. (2005), Laboratory-observed faulting in intrinsically and apparently weak materials: strength, seismic coupling, dilatancy, and pore fluid pressure, this volume.
- Blenkinsop, T. (2000), *Deformation Microstructures and Mechanisms in Minerals and Rocks*, Kluwer Academic Publishers, Dordrecht, 150 pp.
- Bostock, M. G., R. D. Hyndman, S. Rondenay, and S. M. Peacock (2002), An inverted continental Moho and serpentinization of the forearc mantle, *Nature*, *417*, 536-538.
- Bürgmann, R., M. G. Kogan, V. E. Levin, C. H. Scholz, R. W. King, and G. M. Steblov (2001), Rapid aseismic moment release following the 5 December, 1997 Kronosky, Kamchatka, earthquake, *Geophys. Res. Lett.*, *28*(7), 1331-1334.
- Chlieh, M., J.-P. Avouac, V. Hjorleifsdottir, T.-R. A. Song, C. Ji, K. Sieh, A. Sladen, H. Hebert, L. Prawirodirdjo, Y. Bock, and J. Galetzka (2006), Coseismic slip and afterslip of the great (Mw9.15) Sumatra-Andaman earthquake of 2004, *Bull. Seismol. Soc. Am.*, in press.
- Clague, J., and T. S. James (2002), History and isostatic effects of the last ice sheet in southern British Columbia, *Quat. Sci. Rev.*, *21*, 71-87.
- Cohen, S. C. (1984), Postseismic deformation due to subcrustal viscoelastic relaxation

- following dip-slip earthquakes, *J. Geophys. Res.*, *89*, 4538-4544.
- Cohen, S. C. (1994), Evaluation of the importance of model features for cyclic deformation due to dip-slip faulting, *Geophys. J. Int.*, *119*, 831-841.
- Cohen, S. C., and J. T. Freymueller (2001), Crustal uplift in the south central Alaska subduction zone: New analysis and interpretation of tide gauge observations, *J. Geophys. Res.*, *106*(B6), 653-668.
- Davis, D. M., J. Suppe, and F.A. Dahlen (1983), Mechanics of fold-and-thrust belts and accretionary wedges. *J. Geophys. Res.*, *88*, 1153-1172.
- Dixon, T. H. (1993), GPS measurement of relative motion of the Cocos and Caribbean plates and strain accumulation across the Middle America trench, *Geophys. Res. Letters*, *20*, 2167-2170.
- Dragert, H., R. D. Hyndman, G. C. Rogers, and K. Wang (1994), Current deformation and the width of the seismogenic zone of the northern Cascadia subduction thrust, *J. Geophys. Res.*, *99*, 653-668.
- Dragert, H., K. Wang, and T. S. James (2001), A silent slip event on the deeper Cascadia subduction interface, *Science*, *292*, 1525-1528.
- Fialko, Y. (2004), Evidence of fluid-filled upper crust from observations of postseismic deformation due to the 1992 M_w 7.3 Landers earthquake, *J. Geophys. Res.*, *109*, B08401, doi: 10.1029/2004JB002985.
- Flück, P., R. D. Hyndman, and K. Wang (1997), Three-dimensional dislocation model for great earthquakes of the Cascadia subduction zone, *J. Geophys. Res.*, *102*, 539-550.
- Freed, A. M., and R. Bürgmann (2004), Evidence of power-law flow in the Mojave Desert mantle, *Nature*, *430*, 548-551.
- Freed, A. M., R. Bürgmann, E. Calais, and J. Freymueller (2006), Stress-dependent power-law flow in the upper mantle following the 2002 Denali, Alaska, earthquake, *Earth Planet. Sci. Lett.*, *252*, 481-489.
- Freymueller, J. T., and J. Beavan (1999), Absence of strain accumulation in the western Shumagin segment of the Alaska subduction zone, *Geophys. Res. Lett.*, *21*, 3233-3236.
- Freymueller, J. T., S. C. Cohen, and H. J. Fletcher (2000), Spatial variations in continuously monitoring GPS stations about 100 to 250 km from present-day deformation, Kenai Peninsula, Alaska, and their implications, *J. Geophys. Res.*, *105*, 8079-8101.
- Gagnon, K., C. D. Chadwell, and E. Norabuena (2005), Measuring the onset of locking in the Peru–Chile trench with GPS and acoustic measurements, *Nature*, *434*, 205-208.
- Hasegawa, A., N. Uchida, T. Igarashi, T. Matsuzawa, T. Okada, S. Miura and Y. Suwa (2005), Asperities and quasi-static slips on the subducting plate boundary east off Tohoku, NE Japan, this volume.
- Henton, J. A. (2000), GPS Studies of Crustal Deformation in the Northern Cascadia Subduction Zone, Ph.D. thesis, University of Victoria, British Columbia.
- Hsu, Y.-J., M. Simons, J.-P. Avouac, J. Galetzka, K. Sieh, M. Chlieh, D. Natawidjaja, L. Prawirodirdjo, and Y. Bock (2006), Frictional afterslip following the 2005 Nias-Simeulue earthquake, Sumatra, *Science*, *312*, 1921-1926.
- Hyndman, R. D. (2005), The seismogenic zone of subduction thrust faults: What we know and don't know, this volume.

- Hyndman, R. D, and S. M. Peacock (2003), Serpentinization of the forearc mantle, *Earth Planet. Sci. Lett.*, 212, 417-432.
- Hyndman, R. D. and K. Wang (1993), Thermal constraints on the zone of major thrust earthquake failure: The Cascadia subduction zone, *J. Geophys. Res.*, 98, 2039-2060.
- Hyndman, R. D. and K. Wang (1995), Current deformation and thermal constraints on the zone of potential great earthquakes on the Cascadia subduction thrust, *J. Geophys. Res.*, 100, 22,133-22,154.
- Hyodo, M., and K. Hirahara (2003), A viscoelastic model of interseismic strain accumulation in Niigata-Kobe tectonic zone of central Japan, *Earth Planets Space*, 55, 667-675.
- Hu, Y., K. Wang, J. He, J. Klotz, and G. Khazaradze (2004), Three-dimensional viscoelastic finite element model for post-seismic deformation of the great 1960 Chile earthquake, *J. Geophys. Res.*, 109, B12403, doi:10.1029/2004JB003163.
- Igarashi, T., T. Matsuzawa, and A. Hasegawa (2003), Repeating earthquakes and interplate aseismic slip in the northeastern Japan subduction zone, *J. Geophys. Res.*, 108(B5), 2249, doi:10.1029/2002JB001920.
- James, T. S., J. J. Clague, K. Wang, and I. I. Hutchinson (2000), Postglacial rebound at the northern Cascadia subduction zone, *Quart. Sci. Rev.*, 19, 1527-1541.
- Karato, S., and P. Wu (1993), Rheology of the upper mantle: A synthesis, *Science*, 260, 771-778.
- Kato, T., G. S. El-Fiky, and E. N. Oware (1998), Crustal strains in the Japanese islands as deduced from dense GPS array, *Geophys. Res. Lett.*, 25, 3445-3448.
- Khazaradze, G., A. Qamar, and H. Dragert (1999), Tectonic deformation in western Washington from continuous GPS measurements, *Geophys. Res. Lett.*, 26, 3153-3156.
- Khazaradze, G., K. Wang, J. Klotz, Y. Hu, and J. He (2002), Prolonged post-seismic deformation of the 1960 great Chile earthquake and implications for mantle rheology, *Geophys. Res. Lett.*, 29(22), 2050, doi:10.1029/2002GL015986.
- Klotz, J., G. Khazaradze, D. Angermann, C. Reigber, R. Perdomo, and O. Cifuentes (2001), Earthquake cycle dominates contemporary crustal deformation in Central and Southern Andes, *Earth Planet. Sci. Lett.*, 193, 437-446.
- Lay, T., and S. Bilek (2005), Anomalous earthquake ruptures at shallow depths on subduction zone megathrusts, this volume.
- Lay, T., and H. Kanamori (1981), An asperity model of great earthquake sequences, in *Earthquake Prediction: An International Review, Maurice Ewing Ser., Vol. 4*, edited by D. Simpson and P. Richards, AGU, Washington, D. C., pp. 579-592.
- Marone, C., and D. M. Saffer (2005), Fault friction and the upper transition from seismic to aseismic faulting, this volume.
- Masterlark, T., C. Demets, H. F. Wang, O. Sánchez, and J. Stock (2001), Homogeneous vs heterogeneous subduction zone models: Coseismic and postseismic deformation, *Geophys. Res. Lett.*, 28(21), 4047-4050.
- Matsu'ura, M., and T. Iwasaki (1983), Study on coseismic and post-seismic crustal movements associated with the 1923 Kanto earthquake, *Tectonophys.*, 97, 201-215.
- Matsu'ura, M., and T. Sato (1989), A dislocation model for the earthquake cycle at convergent plate boundaries, *Geophys. J. Int.*, 96, 23-32.
- Matsuzawa, T., T. Igarashi, and A. Hasegawa (2002), Characteristic small-earthquake

- sequence off Sanriku, northeastern Honshu, Japan, *Geophys. Res. Lett.*, *29*(11), 1543, doi:10.1029/2001GL014632.
- Mazzotti, S., H. Dragert, R. D. Hyndman, M. M. Miller, and J. A. Henton (2002), GPS deformation in a region of high crustal seismicity: N. Cascadia forearc, *Earth Planet. Sci. Lett.*, *198*, 41-48.
- Mazzotti, S., H. Dragert, J. Henton, M. Schmidt, R. Hyndman, T. James, Y. Lu, and M. Craymer (2003), Current tectonics of northern Cascadia from a decade of GPS measurements, *J. Geophys. Res.*, *108*(B12), 2554, doi: 10.1029/2003JB002653.
- McCaffrey, R. (2002), Crustal block rotations and plate coupling, in *Plate Boundary Zones*, edited by S. Stein and J. Freymueller, AGU Geodynamics Series 30, 101-122.
- McCaffrey, R., M. D. Long, C. Goldfinger, P. C. Zwick, J. L. Nabelek, C. K. Johnson and C. Smith (2000), Rotation and plate coupling along the southern Cascadia subduction zone, *Geophys. Res. Lett.*, *27*, 3117-3120.
- Melbourne, T. I., F. H. Webb, J. M. Stock, and C. Reigber (2002), Rapid postseismic transients in subduction zones from continuous GPS, *J. Geophys. Res.*, *107*(B10), 2241, doi: 10.1029/2001JB000555.
- Melosh, H. J. (1980), Rheology of the earth: Theory and observation, in *Physics of the Earth's Interior, Proceedings of the 1979 Enrico Fermi Summer School, Varenna, Italy*, edited by A. M. Dziewonski and E. Boschi, Noord-Holland, Amsterdam, pp. 318-336.
- Melosh, H. J., and A. Raefsky (1983), Anelastic response of the earth to a dip slip earthquake, *J. Geophys. Res.*, *88*, 515-526.
- Miyashita, K. (1987), A model of plate convergence in Southwest Japan, inferred from levelling data associated with the 1946 Nankaido earthquake, *J. Phys. Earth*, *35*, 449-467.
- Moore, J. C., C. Rowe, and F. Meneghini (2005), How accretionary prisms elucidate seismogenesis in subduction zones, this volume.
- Murray, J., and P. Segall (2002), Testing time-predictable earthquake recurrence by direct measurement of strain accumulation and release, *Nature*, *419*, 287-290.
- Norabuena, E., L. Leffler, A. Mao, T. Dixon, S. Stein, I. S. Sacks, L. Ocola, M. Ellis (1998), Space geodetic observations of Nazca-South America convergence along the Central Andes, *Science*, *279*, 358-362.
- Ozawa, S., M. Murakami, M. Kaidzu, T. Tada, T. Sagiya, Y. Hatanaka, H. Yurai, and T. Nishimura (2002), Detection and monitoring of ongoing aseismic slip in the Tokai region, central Japan, *Science*, *298*, 1009-1012.
- Pacheco, J. F., L. R. Sykes, and C. H. Scholz (1993), Nature of Seismic Coupling Along Simple Plate Boundaries of the Subduction Type, *J. Geophys. Res.*, *98*, 14,133-14,159.
- Peltzer, G., P. Rosen, F. Rogez, and K. Hudnut (1998), Poroelastic rebound along the Landers 1992 earthquake surface rupture, *J. Geophys. Res.*, *103*(B12), 30,131-30,145.
- Piersanti, A. (1999), Postseismic deformation in Chile: Constraints on the asthenospheric viscosity, *Geophys. Res. Lett.*, *26*(20), 3,157-3,160.
- Piersanti, A., G. Spada, and R. Sabadini (1997), Global postseismic rebound of a viscoelastic Earth: Theory for finite faults and application to the 1964 Alaska earthquake, *J. Geophys. Res.*, *102*(B1), 477-492.
- Plafker, G. (1971), Tectonics, in *The Great Alaska Earthquake of 1964: Geology*, pp. 47-

- 122, Natl. Acad. Sci. U. S. A., Washington, D. C.
- Plafker, G. (1972), The Alaskan earthquake of 1964 and Chilean earthquake of 1960 – implications for arc tectonics, *J. Geophys. Res.*, *77*, 901-925.
- Pollitz, F. F. (2003), Transient rheology of the uppermost mantle beneath the Mojave Desert, California, *Earth Planet. Sci. Lett.*, *215*, 89-104.
- Pollitz, F. F., and I. S. Sacks (1997), The 1995 Kobe, Japan, earthquake: A long-delayed aftershock of the offshore 1944 Tonankai and 1946 Nankaido earthquakes, *Bull. Seismol. Soc. Amer.*, *87*, 1-10.
- Pollitz, F. F., R. Bürgmann, and P. Banerjee (2006), Post-seismic relaxation following the great 2004 Sumatra-Andaman earthquake on a compressible self-gravitating Earth, *Geophys. J. Int.*, *167*, 397-420.
- Ranalli, G., and H. H. Schloessin (1989), Role of episodic creep in global mantle deformation, in *Slow Deformation and Transmission of Stress in the Earth, Geophysical Monograph 49*, edited by S. C. Cohen and P. Vanicek, AGU, Washington, D. C., pp. 55-63.
- Rogers, G. C., and H. Dragert (2003), Episodic tremor and slip on the Cascadia subduction zone: The chatter of silent slip, *Science*, *300*, 1942-1943.
- Rydelek, P. A., and I. S. Sacks (1990), Asthenospheric viscosity and stress diffusion: A mechanism to explain correlated earthquakes and surface deformation in NE Japan, *Geophys. J. Int.*, *100*, 39-58.
- Satake, K., K. Wang, and B. F. Atwater (2003), Fault slip and seismic moment of the 1700 Cascadia earthquake inferred from Japanese tsunami descriptions, *J. Geophys. Res.*, *108*(B11), 2535, doi:10.1029/2003JB002521.
- Sato, H., J. T. Freymueller, and S. C. Cohen (2003), 3-D Viscoelastic FEM modeling of postseismic deformation caused by the 1964 Alaska earthquake, southern Alaska, *Eos Trans. AGU*, *84*(46), Fall Meet. Suppl., Abstract G21B-0260.
- Sato, T., and M. Matsu'ura (1992), Cyclic crustal movement, steady uplift of marine terraces, and evolution of the island arc - trench system in Southwest Japan, *Geophys. J. Int.*, *111*, 617-629.
- Savage, J. C. (1983), A dislocation model of strain accumulation and release at a subduction zone. *J. Geophys. Res.*, *88*, 4984-4996.
- Savage, J. C., M. Lisowski, and W. H. Prescott (1991), Strain accumulation in western Washington, *J. Geophys. Res.*, *96*, 14,493-14,507.
- Savage, J. C., J. L. Svarc, and W. H. Prescott (1999), Deformation across the Alaska-Aleutian subduction zone near Kodiak, *Geophys. Res. Lett.*, *26*, 2117-2120.
- Savage, J. C., J. L. Svarc, W. H. Prescott, and M. H. Murray (2000), Deformation across the forearc of the Cascadia subduction zone at Cape Blanco, Oregon, *J. Geophys. Res.*, *105*, 3095-3120.
- Scholz, C. H. (2002), *The mechanics of earthquakes and faulting*, Cambridge University Press, Cambridge, 471 pp.
- Shimazaki, K., and T. Nakada (1980), Time-predictable recurrence model for large earthquakes, *Geophys. Res. Lett.*, *7*, 279-282.
- Stuart, W. D. (1988), Forecast model for great earthquakes at the Nankai Trough subduction zone, *Pure Appl. Geophys.*, *126*, 619-641.
- Suito, H., and K. Hirahara (1999), Simulation of postseismic deformations caused by the 1896 Riku-u earthquake, northeast Japan: Re-evaluation of the viscosity of the upper

- mantle, *Geophys. Res. Lett.*, *26*, 2561-2564.
- Tarantola, A., and B. Vallette (1982), Generalized nonlinear inverse problem solved using the least squares criterion, *Rev. Geophys. Space Phys.*, *20*, 219-232.
- Thatcher, W. (1984), The earthquake deformation cycle at the Nankai Trough, Southwest Japan, *J. Geophys. Res.*, *89*, 3087-3101.
- Thatcher, W., and J. B. Rundle (1984), A viscoelastic coupling model for the cyclic deformation due to periodically repeated earthquakes at subduction zones, *J. Geophys. Res.*, *89*, 7,631-7,640.
- Thatcher, W., T. Matsuda, and J. B. Rundle (1980), Lithospheric loading by the 1896 Riku-u earthquake, northern Japan: Implications for plate flexure and asthenospheric rheology, *J. Geophys. Res.*, *85*, 6429-6435.
- Uchida, N., T. Matsuzawa, and A. Hasegawa (2003), Interplate quasi-static slip off Sanriku, NE Japan, estimated from repeating earthquakes, *Geophys. Res. Lett.*, *30*(15), 1801, doi:10.1029/2003GL017452.
- Ueda, H., M. Ohtake, and H. Sato (2003), Postseismic crustal deformation following the 1993 Hokkaido Niseioki earthquake, northern Japan: Evidence for a low-viscosity zone in the uppermost mantle, *J. Geophys. Res.*, *108*, 2151, doi:10.1029/2002JB002067.
- Wahr, J., and M. Wyss (1980), Interpretation of postseismic deformation with a viscoelastic relaxation model, *J. Geophys. Res.*, *85*, 6471-6477.
- Wang, K. (2000), Stress-strain "paradox", plate coupling, and forearc seismicity at the Cascadia and Nankai subduction zones, *Tectonophysics*, *319*, 321-338.
- Wang, K. (2004), Understanding processes and estimating parameters using mathematical models, in *Hydrogeology of the Oceanic Lithosphere*, edited by E. Davis and H. Elderfield, Cambridge University Press, pp.376-413.
- Wang, K., and J. He (1999), Mechanics of low-stress forearcs: Nankai and Cascadia, *J. Geophys. Res.*, *104*, 15,191-15,205.
- Wang, K., and T. Dixon (2004), "Coupling" Semantics and Science in Earthquake Research, *Eos Trans. AGU*, *85*(18), 4 May.
- Wang, K., and Y. Hu (2006), Accretionary prisms in subduction earthquake cycles: The theory of dynamic Coulomb wedge, *J. Geophys. Res.*, *111*, B06410, doi:10.1029/2005JB004094.
- Wang, K., H. Dragert, and H. J. Melosh (1994), Finite element study of uplift and strain across Vancouver Island, *Can. J. Earth Sci.*, *31*, 1510-1522.
- Wang, K., J. He, H. Dragert, and T. James (2001), Three-dimensional viscoelastic interseismic deformation model for the Cascadia subduction zone, *Earth Planets Space*, *53*, 295-306.
- Wang, K., R. Wells, S. Mazzotti, R. D. Hyndman, and T. Sagiya (2003), A revised dislocation model of interseismic deformation of the Cascadia subduction zone, *J. Geophys. Res.*, *108*(B1), 2009, doi:10.1029/2001JB001227.
- Weertman, J., and J. R. Weertman (1975), High temperature creep of rock and mantle viscosity, *Ann. Rev. Earth Planet. Sci.*, *3*, 293-315.
- Wells, R. E., and R. W. Simpson (2001), Northward migration of the Cascadia forearc in the northwestern U.S. and implications for subduction deformation, *Earth Planets Space*, *53*, 275-283.
- Wells, R. E., C. S. Weaver, and R. J. Blakely (1998), Forearc migration in Cascadia and

- its neotectonic significance, *Geology*, 26, 759-762.
- Williams, C. A., and R. McCaffrey (2001), Stress rates in the central Cascadia subduction zone inferred from an elastic plate model, *Geophys. Res. Lett.*, 28(10), 2125-2128.
- Wolyneec, L. (2004), Improved model constraints for vertical deformation across the northern Cascadia subduction zone, M.Sc. thesis, University of Victoria.
- Wu, P. (1992), Deformation of an incompressible viscoelastic flat earth with power-law creep: a finite element approach, *Geophys. J. Int.*, 108, 35-51.
- Yagi, Y., M. Kikuchi, and T. Nishimura (2003), Co-seismic slip, post-seismic slip, and largest aftershock associated with the 1994 Sanriku-haruka-oki, Japan, earthquake, *Geophys. Res. Lett.*, 30(22), 2177, doi:10.1029/2003GL018189.
- Yoshioka, S., and H. Suzuki (1999), Effects of three-dimensional inhomogeneous viscoelastic structures on postseismic surface deformations associated with the great 1946 Nankaido earthquake, *Pure Appl. Geophys.*, 154, 307-328.
- Yoskioka, S., K. Wang, and S. Mazzotti, Interseismic locking of the plate interface in the northern Cascadia subduction zone, inferred from inversion of GPS data, *Earth Planet. Sci. Lett.*, 231, 239– 247, 2005.
- Zheng, G., R. Dmowska, and J. R. Rice (1996), Modeling earthquake cycles in the Shumagin segment, Alaska, with seismic and geodetic constraints, *J. Geophys. Res.*, 101, 8383-8392.
- Zweck, C., J. T. Freymueller, and S. C. Cohen (2002), Three-dimensional elastic dislocation modeling of the postseismic response to the 1964 Alaska earthquake, *J. Geophys. Res.*, 107, 1-11.

Table 1. Newtonian upper mantle or mantle wedge viscosities used in viscoelastic subduction zone earthquake models.

Subduction Zone	Viscosity (10^{19} Pa s)	Method*	Reference
Aleutian/Alaska	1.2 – 2.2	F-2	<i>Wahr and Wyss</i> [1980]
Alaska	~ 2	F-2	<i>Zheng et al.</i> [1996]
Alaska	1 – 5	A-3	<i>Piersanti et al.</i> [1997]
Cascadia	0.1 – 1	F-2	<i>Wang et al.</i> [1994]
Cascadia	1	F-3	<i>Wang et al.</i> [2001]
Chile	8 – 10	A-3	<i>Piersanti</i> [1999]
Chile	3	F-3	<i>Khazaradze et al.</i> [2002]
Chile	2.5	F-3	<i>Hu et al.</i> [2004]
Nankai	~ 0.5	A-2	<i>Thatcher and Rundle</i> [1984]
Nankai	~ 2	F-2	<i>Miyashita</i> [1987]
Nankai	0.5	A-2	<i>Sato and Matsu'ura</i> [1992]
Nankai	0.8	A-3	<i>Pollitz and Sacks</i> [1997]
Nankai	1	F-3	<i>Yoshioka and Suzuki</i> [1999]
Kanto (Japan)	~ 0.5	A-2	<i>Matsu'ura and Iwasaki</i> [1983]
NE Japan	~ 1	A-2	<i>Thatcher et al.</i> [1980]
NE Japan	~ 1	F-2	<i>Cohen</i> [1984]
NE Japan	0.93	F-3	<i>Suito and Hirahara</i> [1999]
NE Japan	0.7 – 1.3	A-2	<i>Rydelek and Sacks</i> [1990]
NE Japan	0.4	F-3	<i>Ueda et al.</i> [2003]
NE Japan	0.93	F-3	<i>Hyodo and Hirahara</i> [2003]

* F: Finite element; A: Analytical solution; 2: two-dimensional; 3: three-dimensional.

Table 2. Material property values used for the Cascadia viscoelastic model. Poisson's ratio is uniformly 0.25. Rock density is uniformly 3300 kg/m^3 . Gravity is 10 m/s^2 .

Structural Unit	Viscosity (Pa s)	Young's Modulus (GPa)
Continental plate	∞	120
Oceanic plate	∞	120
Continental mantle	10^{19}	160
Oceanic mantle	10^{20}	160

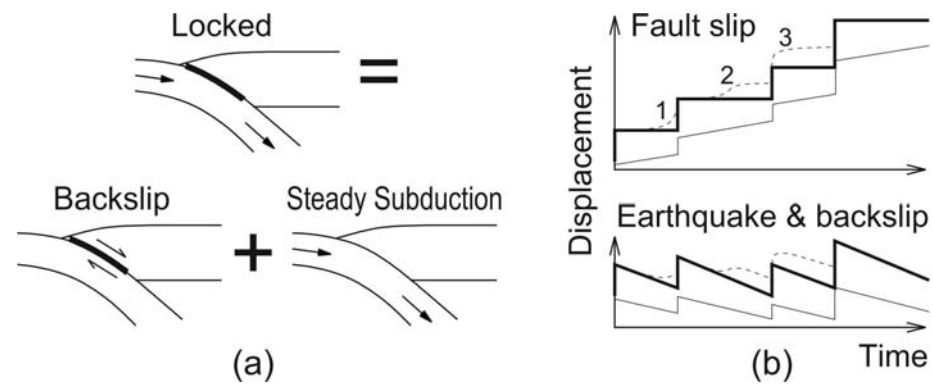


Figure 1. (a) Decomposition of an earthquake cycle problem into a perturbation component and steady subduction component. (b) Schematic illustration of the slip history of a subduction fault including (upper panel) and excluding (lower panel) steady subduction. The thick solid line shows the commonly assumed slip history in earthquake cycle models. The thin solid line is a modification of this history, with the assumption of some constant-rate aseismic slip between earthquakes. Numbered dashed lines represent possible complications of fault slip.

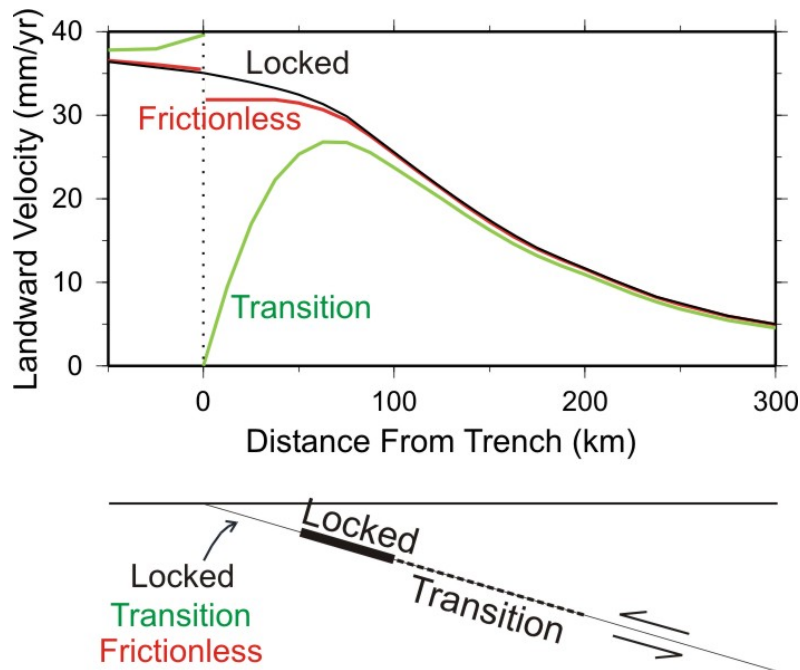


Figure 2. Horizontal surface velocities predicted by three simple 2-D examples with different assumptions (color-coded) on the behavior of the segment updip of the locked zone. Velocities are relative to very remote regions of the upper plate that are not affected by earthquake deformation. The plate convergence rate is 40 mm/yr. Even if the updip segment is frictionless (end member of a very weak fault), it has little interseismic slip because of the presence of the locked zone immediately downdip. The predicted surface velocity (red) is similar to that predicted by assuming the segment to be locked (black). The green curve is the velocity profile if the updip segment is assigned a slip rate that decreases from the plate convergence rate at the trench to zero at the locked zone. Fixing the updip end of the fault at the plate convergence rate (i.e., zero backslip) is a common but possibly incorrect practice in geodetic inversion. Land-based GPS observations usually cannot distinguish between the three models. Because analytical dislocation solutions cannot handle a frictionless fault, these models have been developed using the finite element method. The “locked” and “transition” models reproduce the dislocation solutions almost exactly.

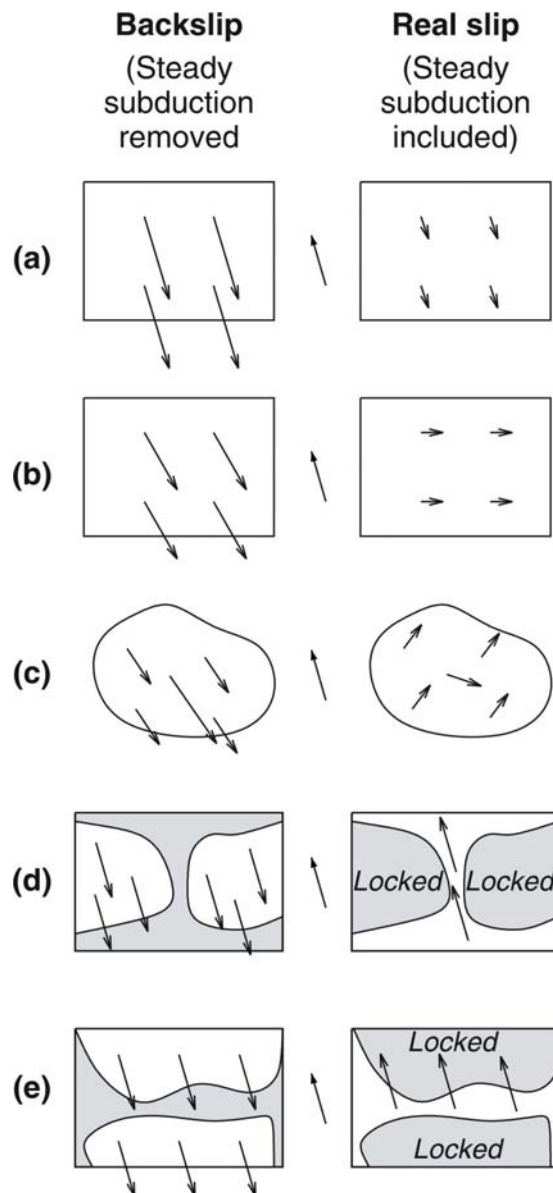


Figure 3. Examples of problematic backslip patterns (left panel) often seen in the literature. The arrows represent slip of the upper plate relative to the lower plate along the plate interface. The arrow in the middle is the steady plate convergence vector. Adding the plate convergence vector to the backslip vectors in the left panel gives the real slip vectors in the right panel.

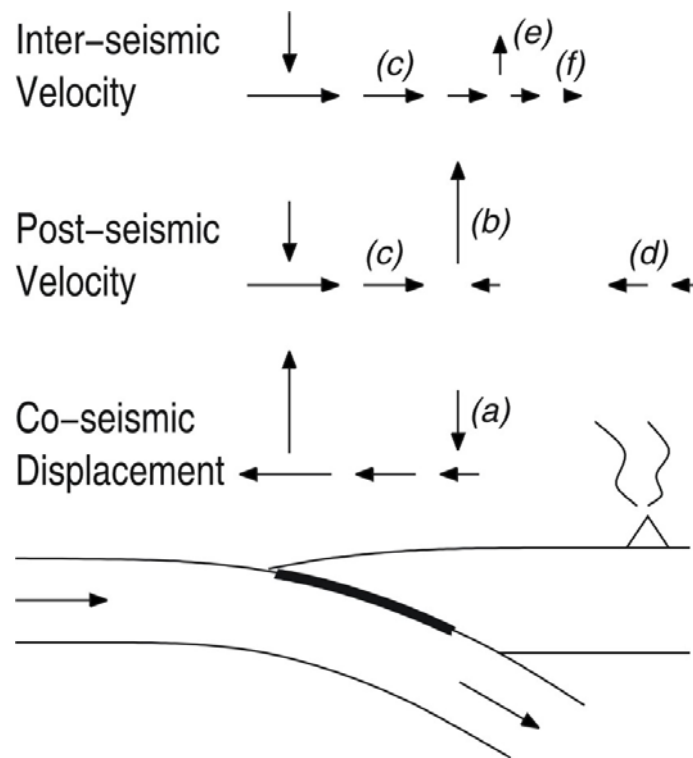


Figure 4. Summary of important features of observed earthquake cycle deformation. For simplicity, co- and postseismic deformation near the trench are not included in this illustration. Here post-seismic indicates a few years to a few decades after a great earthquake, and inter-seismic is a few decades to centuries after the earthquake. See Section 2.2 text for discussion of alphabetically labeled points.

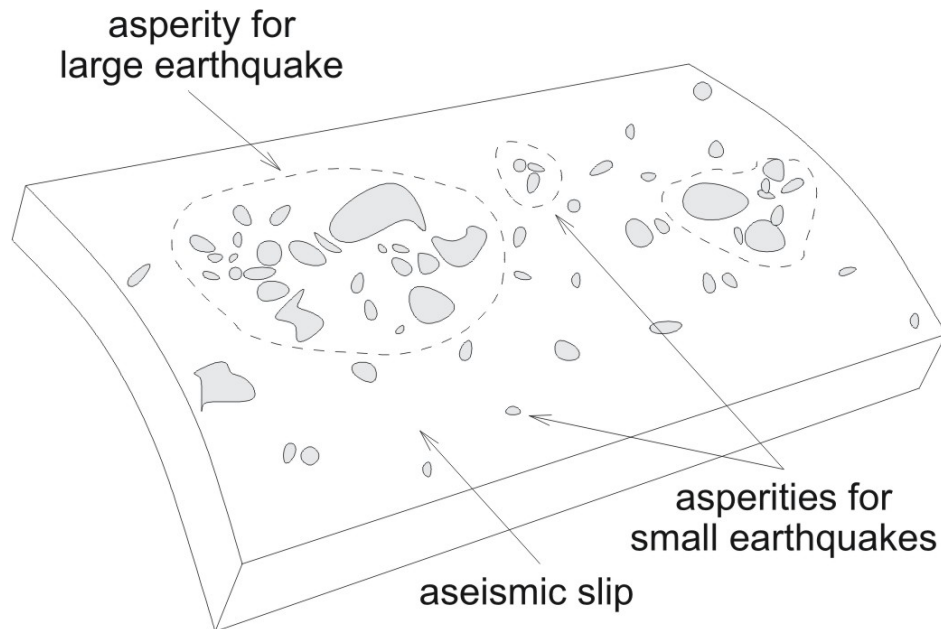


Figure 5. A modification of the conceptual asperity model of *Igarashi et al.* [2003] and *Uchida et al.* [2003]. This is similar to the asperity models of *Lay and Kanamori* [1981] and *Lay and Bilek* (2005), but the fault is envisioned to be a mosaic of stronger and weaker patches at all scales. Closely spaced stronger patches (asperities or groups of asperities) may form a larger asperity. Sparsely spaced asperities or groups of asperities may cause repeating earthquakes.

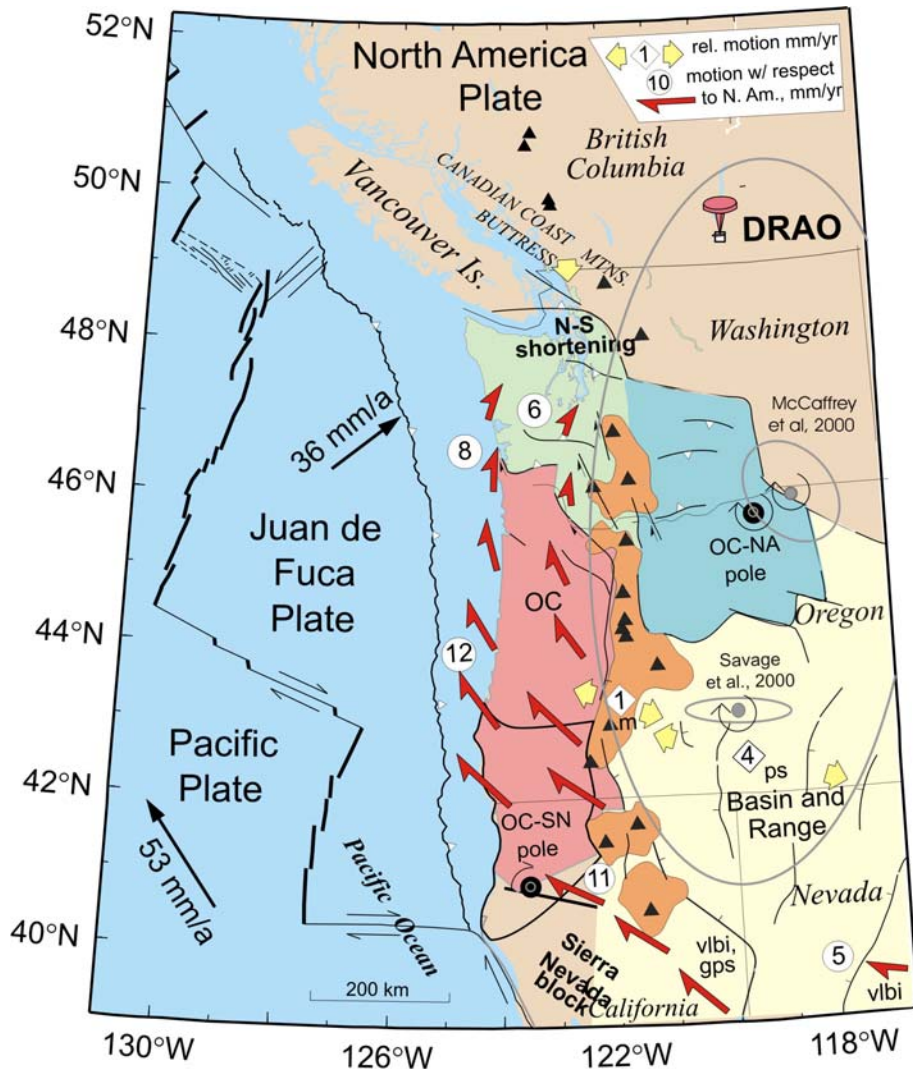


Figure 6. Forearc motion model of *Wells et al.* [1998] and *Wells and Simpson* [2001]. Forearc motion rates (red half arrows) relative to North America (NA) are defined by the OC-NA Euler pole. Rates of motion in mm/yr are given in circles. Oregon block (OC) rotating at Neogene paleomagnetic rate is linked by the OC-SN Euler pole to the Sierra Nevada block (SN), itself rotating about a distant pole at a rate constrained by Very Long Baseline Interferometry (VLBI) and GPS. Poles marked “M” and “S” are OC-NA poles determined using GPS by *McCaffrey et al.* [2000] and *Savage et al.* [2000]. Pairs of yellow arrows indicate relative motion with rates in mm/yr given in diamonds. Where necessary, types of evidence used to constrain motion rates are labeled as follows: ps — paleoseismic, m — paleomagnetic, vlbi — very long baseline interferometry, and gps — global positioning system. The figure is modified from *Wells and Simpson* [2001] by R. Wells. Courtesy of R. Wells.

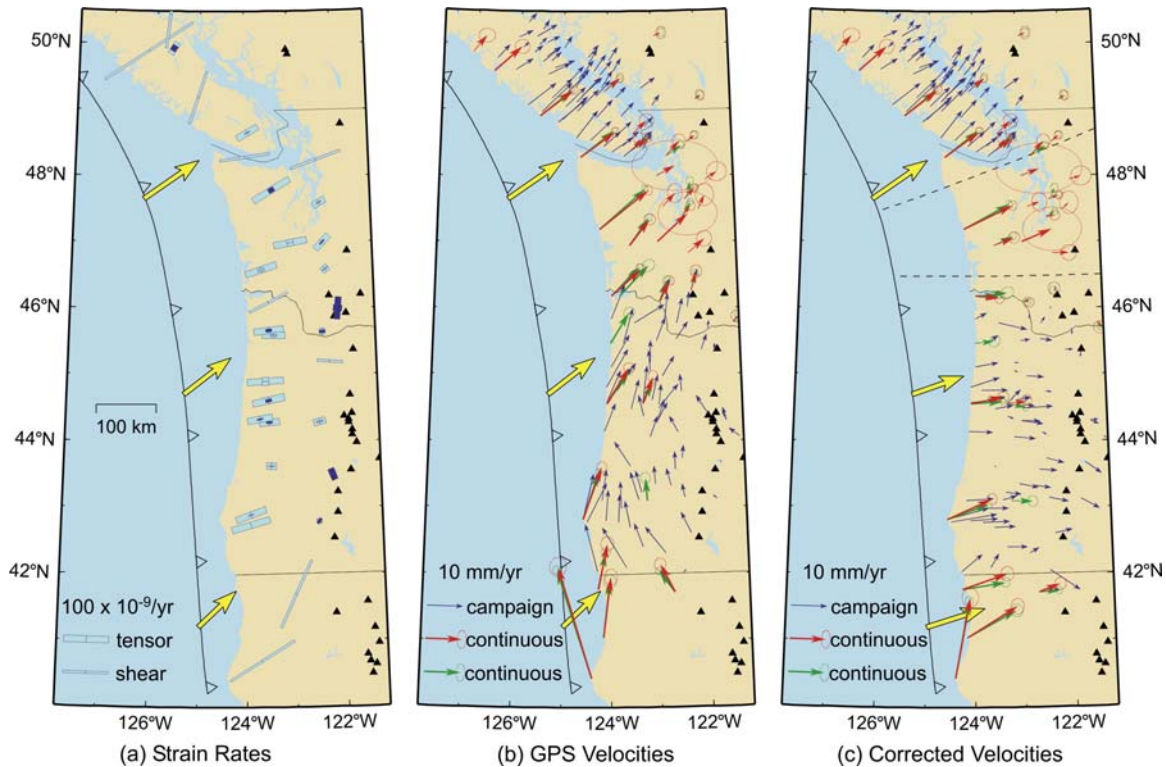


Figure 7. (a) A summary of geodetic strain rate measurements compiled from triangulation, laser ranging, and GPS observations. For strain rate tensor estimates, an open bar indicates contraction, and a solid bar indicates extension. Where only shear strain rates were determined, maximum contraction direction and rate are shown assuming uniaxial contraction. Each value represents an average over the area of the strain network used. (b) GPS velocities relative to reference station DRAO in British Columbia (see Figure 6). Values at continuously monitoring sites determined at the Pacific Geoscience Centre and Central Washington University are shown in red and green, respectively, with the error ellipse representing one standard deviation. (c) GPS velocities after the secular forearc motion shown as red half arrows in Figure 6 is subtracted from sites south of the two dashed lines. No correction is made for velocities north of the dashed lines, and correction applied to sites between the dashed lines is a linear transition. Yellow vectors offshore show the direction of Juan de Fuca plate motion relative to North America in (a) and (b) but relative to Cascadia forearc in (c).

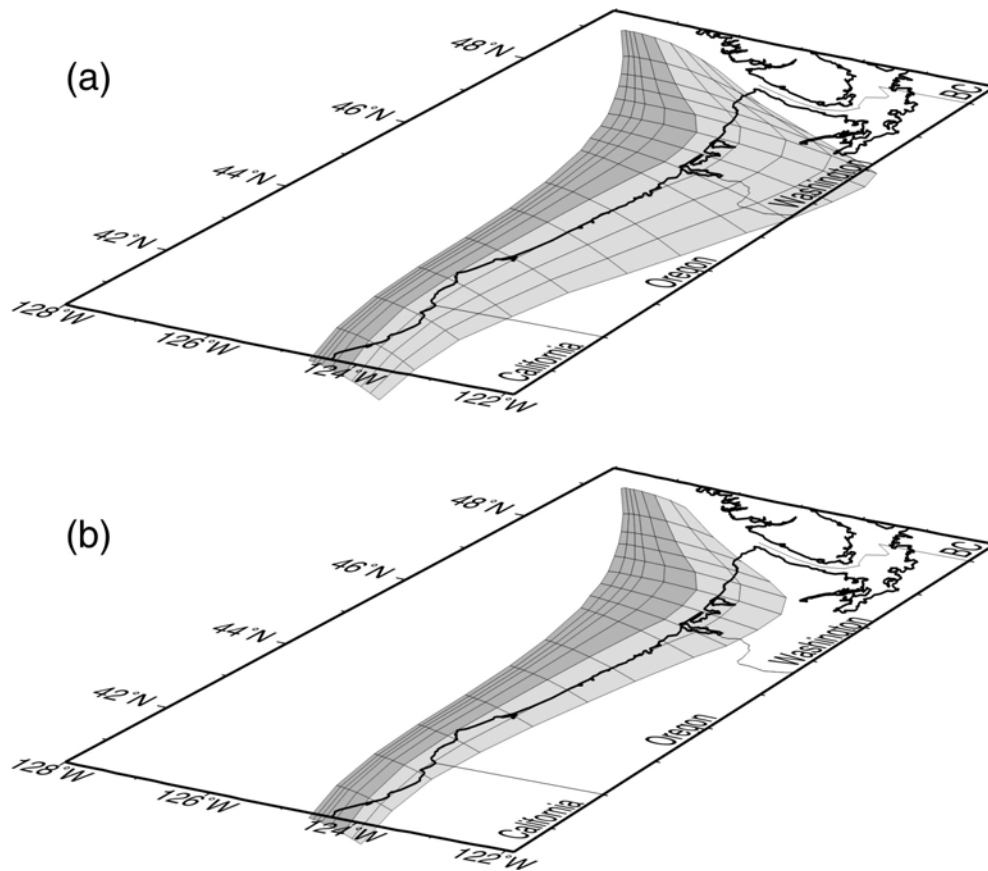


Figure 8. Locked (dark shading) and transition (light shading) zones of the Cascadia margin seismogenic zone used in the elastic dislocation model (a) and viscoelastic finite element model (b).

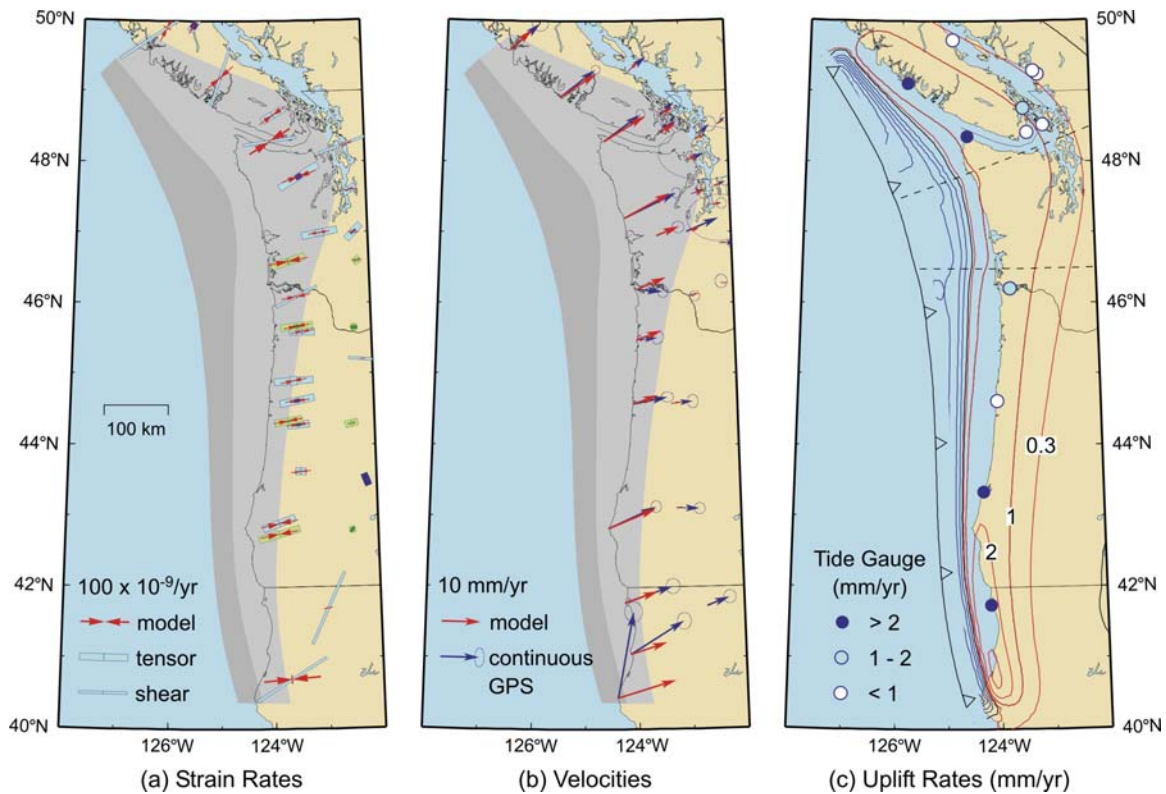


Figure 9. Model results of elastic dislocation model CAS3D-2 compared with geodetic observations. (a) Model and observed strain rates. The “tensor” strain rates are the best geodetic data constraints for an interseismic deformation model. Strain rates reported by *McCaffrey* [2002] (green symbols) were not available as model constraints when CAS3D-2 was developed. (b) Model velocities and continuous GPS velocities. GPS data for central and southern Cascadia have been corrected for secular forearc motion (Figure 6). (c) Model uplift rates (contour lines) and uplift rates derived from tide gauge records. Modified from *Wang et al.* [2003].

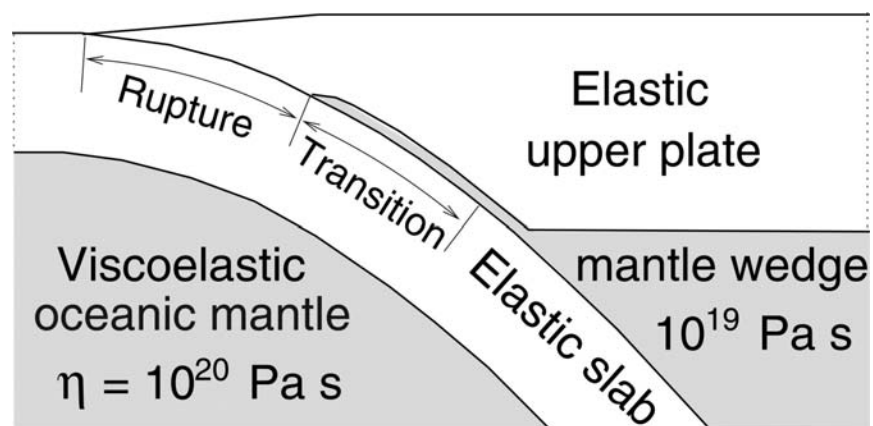


Figure 10. Schematic illustration of the fault structure in the viscoelastic model. The rupture zone is assigned a forward slip to simulate earthquake rupture or a backslip rate to simulate interseismic fault locking. The prescribed slip or backslip rate tapers to zero over the transition zone. The behavior of the transition zone is also controlled by the thin viscoelastic layer along it.

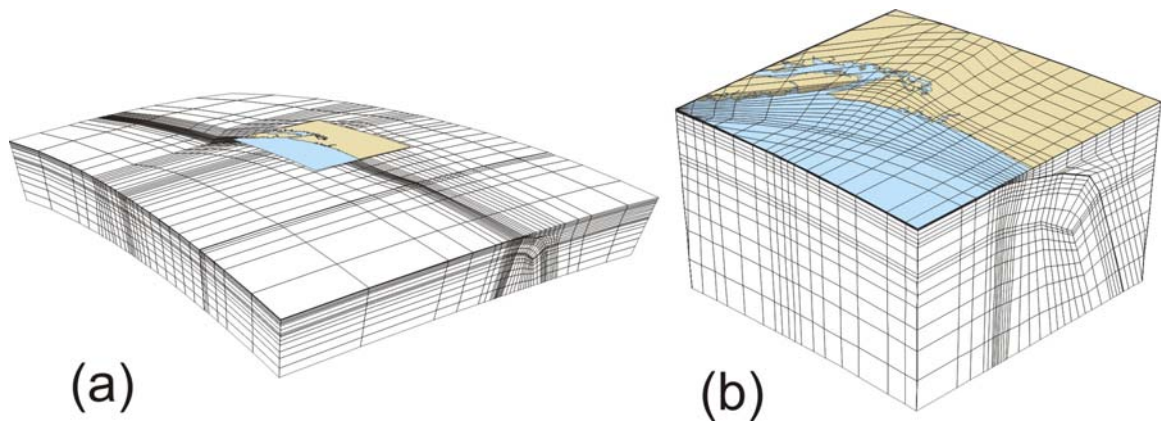


Figure 11. Finite element mesh used for the viscoelastic model for Cascadia. (a) Entire mesh. (b) Detailed view of the colored center portion of (a).

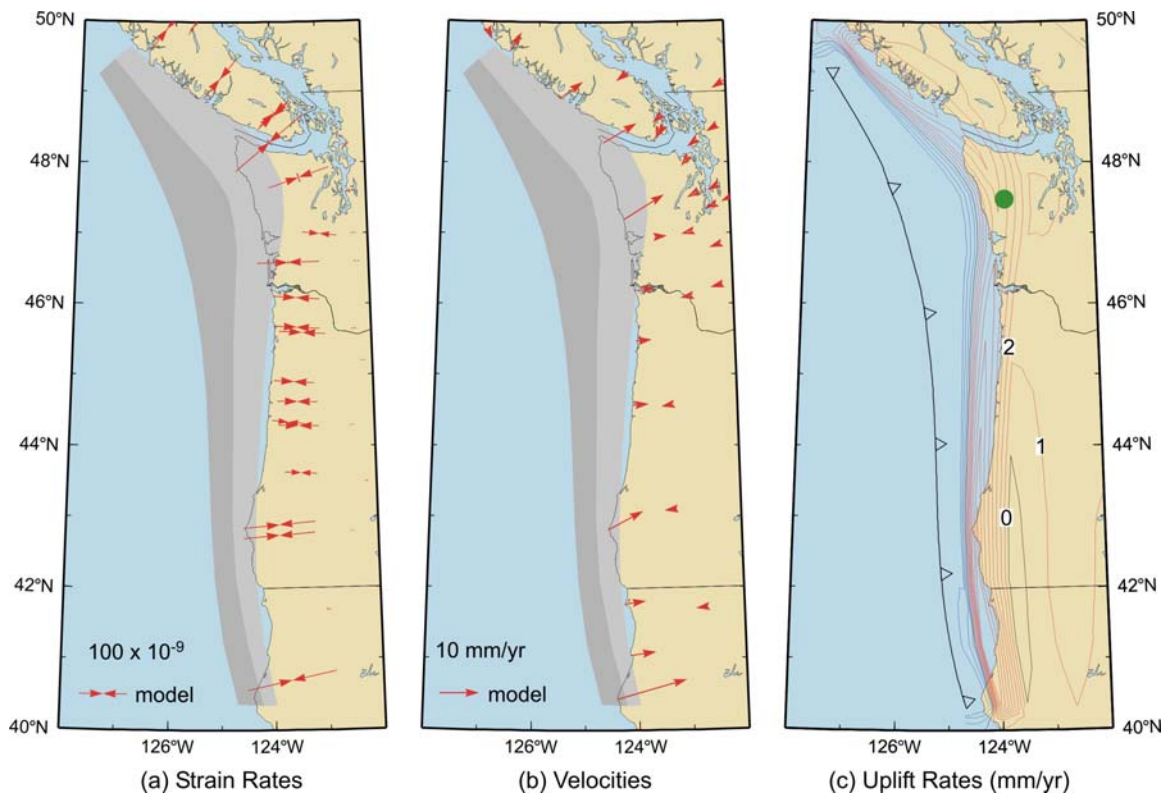


Figure 12. Results of viscoelastic Cascadia model at 50 years after the great earthquake. (a) Strain rates, evaluated at observation points. (b) Velocities, shown only at continuous GPS sites. (c) Uplift rates, contoured at 1 mm/yr interval. Green spot shows the location where uplift history will be displayed in Figure 17.14.

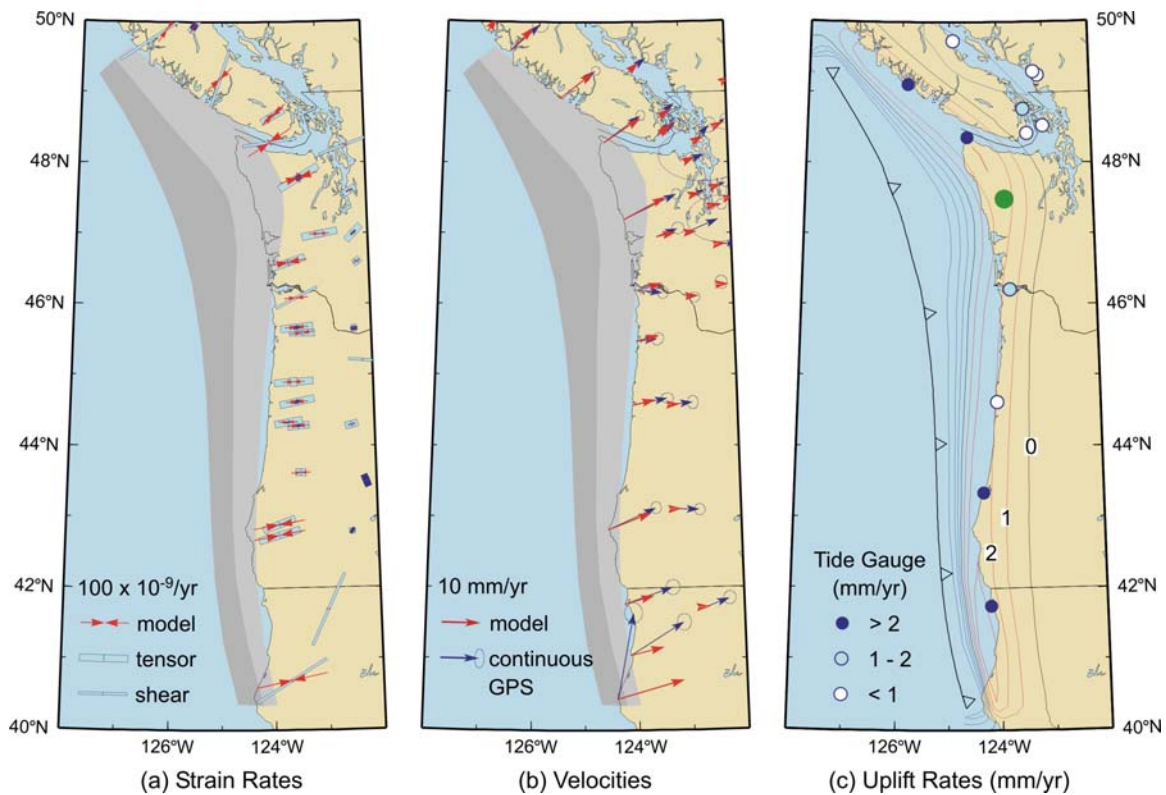


Figure 13. Results of viscoelastic Cascadia model at 300 years after the great earthquake (present) and comparison with geodetic observations. See Figure 7 for explanation of geodetic observations. (a) Strain rates, evaluated at observation points. (b) Velocities, shown only at continuous GPS sites. (c) Uplift rates, contoured at 1 mm/yr interval. Green spot shows the location where uplift history will be displayed in Figure 17.14.

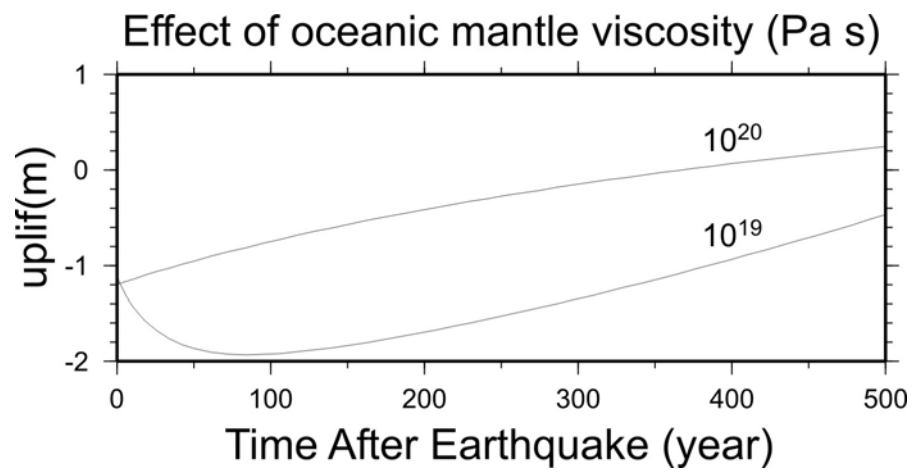


Figure 14. Uplift histories at the location indicated in Figures 12c and 13c by a green spot for models with different oceanic mantle viscosities. The value of 10^{20} Pa s is preferred.